Quantitative Imaging Analysis of Non-Small Cell Lung Cancer

Table of Contents

Acknowledgements

I would like to acknowledge several individuals whose guidance was essential to the completion of this thesis project:

I would like to acknowledge my collaborators and colleagues at the Dana Farber Cancer Institute led by Dr. Hugo Aerts and Dr. Raymond Mak, including Thibaud Coroller, Ying Hou, Elizabeth Hyunh, Vivek Narayan, Patrick Grossman, Stephen Yip, and Emmanuel Rios.

Additionally, I acknowledge funding support from the SMO office at Harvard Medical School.

Abstract

Quantitative imaging is a rapidly growing area of interest within the field of bioinformatics and biomarker discovery. Due to the routine nature of medical imaging, there is an abundance of high-quality imaging linked to clinical and genetic data. This data is particularly relevant for cancer patients who receive routine CT imaging for staging and treatment purposes. However, current analysis of tumor imaging is generally limited to two-dimensional diameter measurements and assessment of anatomic disease spread. This conventional tumor-node-metastasis (TNM) staging system stratifies patients to treatment protocols including decisions regarding adjuvant therapy. Recently there have been several studies suggesting that these images contain additional unique information regarding tumor phenotype that can further aid clinical decision-making.

In this study I aimed to develop the predictive capability of medical imaging. I employed the principles of quantitative imaging and applied them to patients with non-small cell lung cancer (NSCLC). Quantitative imaging, also termed radiomics, seeks to extract thousands of imaging data points related to tumor shape, size and texture. These data points can potentially be consolidated to develop a tumor signature in the same way that a tumor might contain a genetic signature corresponding to mutational burden. To accomplish this I applied radiomics analyses to patients with early and late stage NSCLC and tested these for correlation with both histopathological data as well as clinical outcomes.

Patients with both early and late stage NSCLC were assessed. For locally advanced NSCLC (LA-NSCLC), I analyzed patients treated with preoperative chemoradiation followed by surgical resection. To assess early stage NSCLC, I analyzed patients treated with stereotactic body radiation therapy (SBRT). Quantitative imaging features were extracted from CT imaging obtained prior to chemoradiation and post-chemoradiation prior to surgical resection. For patients who underwent SBRT, quantitative features were extracted from cone-beam CTs (CBCT) at multiple time points during therapy. Univariate and multivariate logistic regression were used to determine association with pathologic response. Concordance-index and Kaplan-Meier analyses were applied to time dependent endpoints of overall survival, locoregional recurrence-free and distant metastasis.

In this study, 127 LA-NSCLC patients were identified and treated with preoperative chemoradiation and surgical resection. 99 SBRT patients were identified in a separate aim of this

study. Reduction of CT-defined tumor volume (OR 1.06 [1.02-1.09], p=0.002) as continuous variables per percentage point was associated with pathologic complete response (pCR) and locoregional recurrence (LRR). Conventional response assessment determined by diameter (p=0.213) was not associated with pCR or any survival endpoints. Seven texture features on pre-treatment tumor imaging were associated with worse pathologic outcome (AUC 0.61-0.66). Quantitative assessment of lymph node burden demonstrated that pre-treatment and post-treatment volumes are significantly associated with both OS and LRR (CI 0.62-0.72). Textural analyses of these lymph nodes further identified 3 unique pre-treatment and 7 unique post-treatment features significantly associated with either LRR, DM or OS. Finally early volume change showed associated with overall survival in CBCT scans of early NSCLC.

Quantitative assessment of NSCLC is thus strongly associated with pathologic response and survival endpoints. In contrast, conventional imaging response assessment was not predictive of pathologic response or survival endpoints. This study demonstrates the novel application of radiomics to lymph node texture, CBCT volume and patients undergoing neoadjuvant therapy for NSCLC. These examples highlight the potential within the rapidly growing field of quantitative imaging to better describe tumor phenotype. These results provide evidence to the growing radioimics literature that there is significant association between imaging, pathology and clinical outcomes. Further exploration will allow for more complete models describing tumor imaging phoentype with clinical outcomes.

Glossary

AUC: Area under the curve
CBCT: cone beam CT
CT: computed tomography
DM/DR: distant metastasis/recurrence
GLCM: gray level co-occurrence matrix
GLSZM: gray level size zone matrix
GRD: Gross residual disease
LoG: Laplacian of Gaussian
LRR: locoregional recurrence
MRD: Microscopic residual disease
MRI: Magnetic resonance imaging
NSCLC: Non-Small Cell Lung Cancer
OS: overall survival
PCA: principal component analysis
pCR: pathologic complete response
PET: positron emission tomography
PLNS: positive lymph node stations
RECIST: Response Evaluation Criteria in Solid Tumors
RLGL: run length gray level
ROC: Receiver operating characteristic
SBRT: Stereotactic body radiation therapy

List of Figures

List of Tables

1. Introduction

1.1 Background

Lung cancer is the cause of the greatest number of cancer related deaths worldwide. In 2010, lung cancer represented 19% of all cancer deaths [1] with a 5-year survival of only 15.9% [2]. Despite efforts to limit risk factors such as tobacco, the global burden of lung cancer is expected to increase in the near future. [3]. The predominant histological subtype of lung cancer is non-small cell lung cancer (NSCLC), which comprises ~80% of lung cancer cases. Within NSCLC, approximately 50% have adenocarcinoma histology and 40% have squamous cell carcinoma [4]. The greatest risk factors for NSCLC is smoking or exposure to tobacco although genetic susceptibility is thought to play a large role in certain populations such as Asian, female, nonsmokers [3,5].

Current standard of care for patients with NSCLC involves the combination of a platinum based chemotherapeutic agent, external beam radiation therapy, and/or surgery [6]. Treatment protocols can vary dramatically based on tumor stage, lymph node involvement and presence of metastases. For example, surgery can be the only treatment modality required for stage I NSCLC. The development of such treatment protocols including those tailored to tumor histology, have resulted in increases in incremental improvements survival compared to historical rates[7]. More recently, there have been numerous advances in targeted and immune-based therapies [8,9].

Targeted therapies are directed towards specific mutations within oncogenic proteins. Mutations within the genes KRAS, EGFR, ALK, and BRAF are the most commonly identified in NSCLC, with KRAS and EGFR making up approximately 30% of adenocarcinoma mutations. The EGFR inhibitors erlotinib and gefitinib are examples of therapies that have successfully targeted an oncogenic mutation [10]. However, not all mutations show benefit to targeted inhibition. For example, KRAS mutations are found in approximately 20% of NSCLC patients and are mutually exclusive of EGFR mutations. KRAS mutations are associated with a poor prognosis [11] however attempts to inhibit KRAS have not shown significant benefit to date [12]. Similarly, while p53 mutations are associated with worse prognosis [13], these mutations have not emerged as targets for therapy. Additionally, since patients who respond to targeted

therapies for EGFR and ALK inevitably acquire resistance [14,15], there is need for improved methods of tumor surveillance even for patients who have known genetic mutations.

Thus, despite advances in the genomic characterization of tumors, improving survival continues to remain challenging for a significant proportion of NSCLC patients. Although the development of novel therapeutics will remain an important priority and cornerstone of cancer treatment, there is a concomitant need for better prognostic tools to assess therapeutic response, monitor tumor progression, and predict clinical outcomes. Such tools could better stratify patients to optimal treatment protocols based on risk and eventually lead to more individualized treatment regimens. This goal has led to the aim of improving non-invasive methods of describing tumor phenotype including serum biomarkers, circulating tumor cells and medical imaging [16–18]. These non-invasive methods provide alternatives to the more invasive process of obtaining tissue directly from the tumor. Quantitative imaging seeks to be one of these non-invasive methods that can predict tumor behavior. In this study I explore the association between quantitative imaging and clinical outcomes.

1.2 Tumor response imaging

1.2.1 Imaging for conventional treatment delivery

Tumor imaging is a standard component of clinical staging algorithms for the treatment of NSCLC. CT and PET imaging are typically used to determine the size of the primary tumor, extent of nodal involvement, and metastatic spread. After staging, imaging is used to monitor tumor response during therapy. Such imaging essentially acts as a non-invasive surrogate for histopathology since pathologic response is only available at the time of surgery or biopsy. The imaging modalities typically used for tumor response assessment are either CT or PET imaging. There are multiple methods for evaluating tumor response but the most commonly used criteria (including for clinical trials) is Response Evaluation Criteria in Solid Tumors (RECIST). RECIST is a standardized framework for measuring solid tumor size and determining response [19,20]. These criteria are based on the sum of the diameters of lesions but do not provide guidance for the use of advanced imaging features. RECIST response groups patients into complete response (CR), partial response (PR), stable disease (SD) or progressive disease (PD). A partial response is a reduction in tumor diameter between 30-100%, with 100% reduction being a complete response. However, few studies have demonstrated an association between RECIST response and survival since the initial guidelines were published [19–21], and there are

few guidelines as to the utility of RECIST partial response in clinical decision-making for NSCLC.

Prior imaging studies of NSCLC have described pre-treatment tumor volume as a prognostic factor [22,23] or evaluated more advanced imaging features including FDG uptake, volume reduction, and texture as predictors for response to therapy [24–28]. Despite the prognostic significant of volume or FDG uptake, it is unclear if a response on imaging truly correlates to tumor response on pathology. William et al have previously noted a high rate of discordance between RECIST response and pathologic response [29]. Further assessment of radiopathologic correlation is difficult given the lack of studies examining this relationship. However, it is becoming more apparent that there is value to understanding pathological outcome. Multiple studies have demonstrated a correlation between pathologic response and survival [30–34] suggesting that prediction of pathologic response can act as a surrogate endpoint for survival.

1.2.2 Imaging for Stereotactic body radiation therapy

Stereotactic body radiation therapy (SBRT) is a growing treatment option for the delivery of radiation therapy to a wide variety of tumors including lung cancer [35]. SBRT involves the delivery of higher doses of radiation over a smaller number of doses (fractions). This has been enabled by the development of highly conformal radiation delivery that reduce toxicity to surrounding tissue. For lung cancer patients, SBRT is typically used for early stage disease as an alternative to surgical resection [36–38]. Given the recent application of this form of fractionation, it remains an active area of interest for the development of prognostic indictors for response to radiation therapy.

Current prognostic indictors for use in SBRT typically are typically composed of clinical factors such as number of lesions, gender and performance status [39]. There has additionally been development of biomarkers such as cell free DNA [40]. Of particular interest, would be to use to predict response during treatment, as a means of adjusting the dose delivered during each treatment or the area to be treated. This is particularly challenging given the short duration of treatment for which it may be more difficult to obtain clinically valuable information.

The use of imaging for prognostic purposes in SBRT for NSCLC has been limited. Matsuo et al demonstrated that tumor diameter was associated with overall survival [41].

Existing literature suggests that the use of cone beam CT can offer texture based analysis that is robust but highly dependent on imaging protocol and motion [42].

1.3 Radiomics

1.3.1 Overview of Radiomics

Radiomics is an emerging field that assigns quantitative values to features extracted from medical imaging. These features capture imaging traits unable to be appreciated by the human eye including intensity level, spatial relationships between areas of differential intensity, shape and texture. Radiomics complements work describing qualitative or semi-quantitative forms of image analysis such as pleural attachment or spiculations [43]. The process of obtaining radiomics data from medical imaging occurs in the following steps 1) image acquisition 2) tumor identification and anatomic delineation (segmentation) manually or automated [44] 3) feature extraction 4) data analysis [45].

Radiomic features can be grouped into first order statistics, shape and size based features, and textural features. First order statistics describe voxel distribution within the tumor such as the mean or median voxel intensity. Features such as skewness or kurtosis similarly describe the histogram of voxel intensities. Shape and size based features include diameter, volume, surface area and sphericity [46,47]. Additional manipulations of the data include the application of filters such as Laplacian of Gaussian (LoG) and wavelet that have been previously described in other applications of non-medical image analysis [48,49]. The wavelet filter decomposes the information within the image such that only low or high intensity information is analyzed. The LoG filter is sensitive to edge detection and can also eliminate noise within the image. Radiomics has repurposed these imaging tools for use in a clinical context.

1.3.2 Clinical applications of Radiomics

In terms of clinical utility, radiomics platforms have already been developed for multiple imaging modalities including CT, PET and MRI. [50,51]. These platforms have been utilized to describe a variety of malignancies including head and neck, lung [46], glioblastoma [52], sarcoma [53] and prostate cancer [54]. There are multiple potential applications of radiomics. Textural features can be used to determine if a suspicious imaging finding represent malignancy. Andersen et al demonstrated that texture features can distinguish between benign and malignant lymph node involvement in lung cancer patients [55]. Similarly, in prostate cancer, texture

features have been shown to be able to distinguish malignancy from normal tissue [56] and thus aid in prostate cancer detection [57].

Another application is in the use as a prognostic biomarker. Lubner et al previously demonstrated the correlation between textural features and overall survival in hepatic metastatic colorectal cancer [58]. Cunliffe et al demonstrated association between radiomics features and toxicity resulting in radiation pneumonitis [59]. Coroller et al found that textural features of primary NSCLC tumors are associated with prediction of distant metastases [60].

Finally, an intriguing application of quantitative imaging is treatment monitoring and response prediction. The utility of radiomics may not only be limited to risk stratification, but may also be used for longitudinal treatment monitoring and surveillance along with PET/CT/MRI imaging modalities. For example, Cook et al describe the use of PET texture correlated with RECIST response in NSCLC patients treated with erlotinib [61].

1.4 Rationale

As outlined above, genetic and clinical information offer significant benefit to the understanding of tumor phenotype. However, there is increasing evidence that tumor architecture as dissected by quantitative imaging can offer additional, complementary information to routinely obtain clinical or genetic data. In this work, I sought to apply the principles of quantitative imaging to NSCLC lung cancer patients. These patients offer many benefits that make them suitable for studies in quantitative imaging. Unlike prostate, ovarian, or colon cancer, there are currently no serum markers that are clinically used for assessing tumor burden, severity or response to therapy for patients with NSCLC. These patients thus undergo regular surveillance imaging. Additionally, given that radiation therapy can be a primary treatment modality for both early and late stage NSCLC, patients routinely undergo high quality CT scans during treatment planning. Finally, these patients have a high event rate of local recurrence, distant metastases and death that facilitates the study of clinical endpoints. On the other hand, lung cancer patients often have poor image quality due to artifact and motion from breathing that limits the information that can be gathered. I hypothesize that applying quantitative data mining techniques to images obtained clinically can describe the tumor phenotype for NSCLC and will be predictive for pathological and clinical outcomes.

2. Materials and Methods

2.1 Patient Identification

The study was conducted under an IRB approved protocol. Retrospective analysis identified 127 patients who underwent chemoradiation followed by surgical resection between 2001-2013 at Brigham and Women's Hospital/Dana Farber Cancer Institute. 101 of these patients had CT imaging available for analysis at both the initiation and completion of radiotherapy prior to surgical resection. For analysis of CBCT images, an additional 99 patients who underwent SBRT between 2009-2013 were identified.

Pathology reports at the time of surgical resection provided pathologic restaging. At our institution, residual tumor is indicated as either gross residual disease (GRD) or microscopoic residual disease (MRD). Complete tumor eradication was considered a pathologic complete response (pCR).

Exclusion criteria included delayed surgery greater than 120 days after the completion of radiotherapy, presence of distant metastases (Stage IV) at diagnosis or prior to planned resection, and CT imaging with slice thickness greater than 5.0 mm. Patients without gross tumor volume (GTV) or clinical target volume (CTV) contours from the treating radiation oncologist were excluded from this study.

2.2 CT Acquisition

Planning CTs were acquired according to scanning protocol at our institution using GE "Lightspeed" CT scanner (GE Medical System, Milwaukee, WI, USA).

2.3 Tumor Segmentation

Tumors were segmented on CT scans obtained both before (pre-treatment) and after radiation therapy (post-treatment). Original planning CT scans and tumor contours were retrieved from Eclipse Treatment Planning System (Varian, Palo Alto, CA). Post-treatment volumes were contoured on diagnostic CT scans obtained clinically for re-staging prior to surgery. Pre-treatment volumes were registered to post-treatment CT images using deformable registration via MIM Maestro (MIM Software Inc., Cleveland, OH) to guide post-treatment contouring. Where clinically involved nodal stations were clearly demarcated from the primary tumor, a separate contour was created for primary tumor measurements.

For patients undergoing SBRT, cone-beam CT scans (CBCTs) were obtained at the first and last radiotherapy treatment date. A third CBCT scan was obtained at the mid-point of

treatment regardless of the number of radiation fractions prescribed. Original planning tumor contours were reviewed for tumor identification and segmentation guidance. Tumors were segmented on CBCT images using Eclipse Treatment Planning System (Varian, Palo Alto, CA).

All contours were modified to exclude air, blood vessels, and normal tissue, and subsequently reviewed by an attending radiation oncologist.

2.4 Radiomic feature extraction

A set of 1605 radiomic features describing the tumor phenotype was extracted using an in-house Matlab 2013 (The Mathworks Inc., Natick, MA, USA) toolbox and 3D Slicer 4.4.0 software [62]. All CT voxels were resampled to 3 x 3 x 3 mm3 prior to feature extraction to standardize the voxel spacing across the cohort. (**Figure 1**) A standard bin width of 25 Hounsfield units (HU) was used for textural features. These features were organized into discrete categories including shape, statistics and textural features **(Figure 2, Table 1)** [46]. Laplacian of Gausiann (LoG) and wavelet filter were subsequently applied to extracted features to obtain additional features corresponding to discrete intensity bands.

After extraction of radiomic features, principal component analysis (PCA) was applied to the feature set using the FactoMineR package for R software. PCA reduction of the feature set allowed for independent selection of a limited number of features to then test prognostic value. Imaging features were thus selected for the maximal representation of the feature set without consideration of study endpoints. Features retaining 95% of the variability and 99% of the correlation to PCA scores were selected for further analysis.

2.5 Tumor Size Calculations

Volume and diameter measurements were performed by MIM Maestro and Eclipse treatment planning system. Relative changes in tumor volume or diameter were calculated as $\%(\text{Tumor}_{\text{post-treatment}} - \text{Tumor}_{\text{pre-treatment}})/\text{Tumor}_{\text{pre-treatment}}$ as previously described [63].For CBCT volumes, relative changes were calculated using combinations of two out of three treatment volumes extracted. Rate of change was calculated using the slope of decrease between any two imaging time points. Volume measurements are reported in cubic centimeters for the sum total tumor volume including the primary tumor and all clinically involved lymph nodes.

Uni-dimensional diameters were measured according to RECIST 1.1 guidelines [20]. Diameters are reported in centimeters for the sum total tumor diameter. A maximum of 5 total

lesions were included in diameter calculations. Primary tumors less than 1.0 cm in the long axis and lymph nodes less than 1.5 cm in the short axis were excluded per RECIST 1.1 guidelines.

2.6 Outcomes

Survival outcomes were locoregional recurrence (LRR), distant metastasis (DM), and overall survival (OS). Locoregional recurrence was defined as recurrence at the resection site, hilar nodes, mediastinal nodes, or supraclavicular nodes. All other sites were defined as distant metastasis. LRR and DM were defined as the time interval from the date of surgery until the first radiographically evident locoregional recurrence or distant metastasis respectively, and censored at the date of last negative re-staging scans in patients without recurrence. OS was defined as the time from the date of surgery until death from any cause, and censored at the last date of follow-up.

2.7 Statistical Analysis

All statistical analyses were performed using SAS version 9.4 (SAS Institute, Cary, NC) and R software version 3.2.2 using the survcomp package version 1.16 from Bioconductor.

Univariate and multivariate logistic regression with stepwise selection were used to identify clinical or imaging features associated with pathologic complete response. Log-rank test and Kaplan-Meier analyses were utilized to analyze time-dependent variables including LRR, DM, and OS. Multivariate survival analysis was performed using the Cox proportional hazards model with stepwise selection. Receiver operating characteristic (ROC) curves were calculated to identify the performance of continuous imaging variables [63].Comparison of ROC areas under the curve (AUC) was performed as described by DeLong et al [64]. Optimal cutoff for sensitivity and specificity was derived from the ROC curve using the Youden index (J) [65].

The prognostic performance of the imaging features was evaluated by calculating the concordance index (CI). The CI is a generalization of the time dependent area under the receiver operating characteristic curve (AUC). The CI is a measure of the probability that between two randomly drawn samples, the sample with the higher value (e.g. of an imaging feature) will have a higher likelihood of the event. A CI greater than 0.5 indicates direct proportionality between the feature value and clinical outcome whereas a CI less than 0.5 indicates inverse proportionality to the event. A CI of 0.5 indicates no association between the feature and the outcome. The Noether test was used to compute the p-value to determine the significance of the

CI from random (CI = 0.5). Statistical significance from random CIs was calculated using the "survcomp" package. P-values less than 0.05 were considered significant.

3. Results

3.1 Size-based metrics for locally advanced NSCLC

Clinical trials and treatment plans typically use tumor diameter for assessing response or progression. Since diameter is a conventional metric of response, I sought to more clearly elucidate the relationship of imaging measurements of tumor size with pathological response, given that pathological response is a direct measure of the tumor response to therapy. A decrease in tumor diameter of 30% or more is considered a response to therapy based on standard RECIST criteria. Tumors are considered stable or progressing if they do not shrink at this cut-off. However, there are surprisingly few studies that have validated additional quantitative size-based metrics with regard pathologic response or clinical outcomes.

3.1.1 Patient characteristics and outcomes

In order to evaluate the effect of sized based changes, I retrospectively analyzed 101 patients with NSCLC who underwent neoadjuvant chemoradiation prior to surgical resection. The median age of patients was 60 years (range 32-77) at the time of diagnosis. Patient and treatment characteristics are shown in **Table 2**. The majority of patients presented with adenocarcinoma (57.4%) or squamous cell carcinoma (26.7%) histology. The median preoperative radiation dose was 54 Gy, and 98% of patients received concurrent chemotherapy. The median time from the completion of chemoradiation to the first post-treatment scan was 18 days (Range 0-92), and the median time from chemoradiation to surgery was 44 days (Range 21-119). 81 patients (80.1%) had residual disease and 20 patients (19.8%) had a pCR at the time of surgery.

Patient outcomes are shown in **Table 3**. Median follow up was 36 months, (range 0.4-113 months). Median overall survival was 60.1 months. The 3-year estimates of locoregional recurrence, distant metastases and OS were 25%, 37%, and 64% respectively

3.1.2 CT Volume and Diameter Changes in Patients with pCR

The median relative change in CT measured tumor diameter was -26.6% (Range -100 to +49.3%). The median relative change in tumor volume was -50.5% (Range -90.9 to +185.2%).

Figure 3 summarizes tumor response utilizing a waterfall plot for each patient based on the percent change in tumor diameter (**3a**) and volume (**3c**) grouped by pathologic response. For patients with pCR and residual disease, the median change in volume was -60.3% (Range -81.9 to -35.8%) and -41.9% (Range -90.9, +185.2%) respectively. The median change in diameter was -41.1% (Range -100.0 to +3.7%) and -24.4% (Range -63.1 to +49.4%) for pCR and residual disease respectively (**Figure 3b, 3d**). The decrease in tumor volume and diameter (p=0.02) was significantly higher in patients with pCR compared to residual disease (p<0.001, Wilcoxon rank sum test).

3.1.3 Univariate and Multivariate Analysis

Univariate logistic regression further demonstrated association between pCR and change in tumor volume (OR 1.06, 95% CI [1.02-1.09], p=0.002) as well as tumor diameter per percentage point (OR 1.04, 95% CI [1.01-1.06], p=0.006). Notably, there was no association between pCR and absolute tumor size. This was true for tumor size both prior to and after chemoradiation. Examining clinical variables, N0 status, squamous cell histology, and number of positive lymph node stations (PLNS) at diagnosis were significantly associated with pCR (**Table 4**). Age, performance status, race, gender, Stage and radiation dose did not have a significant association.

All factors significant for pathologic complete response on univariate analysis were entered into a multivariate logistic model. Tumor volume decrease remained an independent predictor of pathologic response in the multivariate analysis (OR:1.08, 95%CI:[1.03-1.13], p=0.002) in addition to N2/N3 Stage (OR:0.18, 95%CI:[0.05-0.62] p= 0.001) and histology sub-type.

3.1.4 RECIST Response does not predict pCR

Given the association between volume/diameter changes and pCR, existing imaging response criteria (RECIST) were compared with pathologic response. Using RECIST response threshold of 30% decrease in tumor size, there were 43 (42.6%) patients with a RECIST complete or partial response (CR/PR) and 58 (57.4%) patients with stable or progressive disease (SD/PD) (**Table 3**).

RECIST CR/PR versus SD/PD had no association with pCR on unviariate logistic regression (p= 0.21). The sensitivity and specificity of RECIST response for predicting pCR was 55% and 60% respectively.

3.1.5 Receiver Operating Characteristics

To further quantify the efficacy of the discovery model using imaging size with pathologic response, I generated ROC curves for univariate CT imaging models predicting pCR. Relative change in volume had an AUC of 0.76 compared to AUC of 0.67 for relative change in tumor diameter (**Figure 4**). Both volume and diameter models were significant from random ($p<0.05$). The optimized volumetric cutoff was 54.6% decrease in volume resulting in 85% sensitivity and 64.2% specificity.

The optimal point for predicting pCR using change in diameter was 47.6% decrease, resulting in 40% sensitivity and 87.7% specificity. Changes in primary tumor volume and change in primary tumor diameter were analyzed separately and were also significantly associated with pCR. No other imaging characteristics reached significance.

3.1.6 Timing of Imaging does not Affect Univariate Predictions

The median duration between pre-treatment and post-treatment CT imaging was 70 days (range 35-159). To account for variability in early tumor response, I performed subgroup analysis of patients with early (<70 days) and late CT imaging (>70 days). Pathologic response was correlated to tumor volume decrease per percentage point in both patients with earlier scans ($p=0.01$) and late scans ($p=0.04$). Furthermore, the average percent changes per day in volume and diameter was also associated with pCR. The median tumor volume change per day was -0.73% (Range -1.61 to +2.64%) and the median diameter change per day was -0.39% (Range -1.27 to +0.71%). Both percent decrease of tumor volume change per day (OR 9.14, 95% CI [1.53-54.81] $p=0.02$) and diameter (OR 5.76, 95% CI [1.20-27.6] $p=0.03$) remained significantly associated with complete pathologic response.

3.1.7 Survival Outcomes Analyses

Given the association between volume/diameter changes and pathologic response, I also tested the association between survival and imaging response. Volume change, diameter change, and RECIST response were not associated with LRR, DM, or OS. However, patients with less advanced stage IIA-IIIA disease had greater LRR than IIIB disease (3 year freedom from LRR 78.8% [67.0- 86.8%] vs 47.9% [17.5-73.2%], $p=0.04$).

3.1.8 Stage IIIA Subgroup Analysis

Since trimodality therapy and questions regarding optimal therapies for local control are particularly controversial for stage IIIA patients, I performed a subgroup analysis of only stage

IIIA patients (n=77). The median change in volume for this subgroup was -48.3% (Range -83.6 to 185.2%). The median change in diameter was -27.9% (-100 to 49.4%). Similar to the results obtained from analysis of the entire cohort, there was an association between percent tumor volume decrease (p=0.002) and percent tumor diameter (p=0.001) decrease with pCR in stage IIIA patients.

I then examined survival outcomes. There was no association between imaging changes and OS or DM. However, in the subgroup analysis of stage IIIA patients, total change in volume was associated with locoregional-recurrence (p=0.0367). Using the median volume change of – 48.3% as a cutoff, patients with greater volumetric decrease had decreased LRR compared to patients with smaller volumetric decreases (**Figure 5a**). In contrast, there was no association between RECIST response and LRR (**Figure 5b**).

3.2 Shape and Texture based features predict pathologic response

Since volumetric changes were able to predict pathologic response and local recurrence with greater efficacy than conventional 2-dimensional diameter measurements, I reasoned that higher order features could similarly predict pathologic and survival outcomes. In order to better identify textural features associated with clinical outcomes, I applied radiomics analysis to CT images obtained prior to therapy. The goal of such an analysis would be to predict patients at higher risk of poor response prior to the initiation of therapy. Such analyses could then logically extend to imaging obtained during therapy or after the completion of therapy.

3.2.1 Patient characteristics and outcomes

127 patients with NSCLC were included in this study. The median age was 60.5 years old (range 32.7 to 77.6). Tumor histology was predominantly adenocarcinoma (56.6%) and AJCC stage IIIA (75.6%). The median follow-up was 41.8 months. Pathologic response was 27 (21.3%) complete response, 33 (26.0%) microscopic disease and 67 (52.7%) gross residual disease (**Table 5)**. The median time for OS, DM, and LRR was respectively 41.8, 24.8, and 28.1 months. (**Table 6)**.

3.2.2 Radiomics predicts pathologic response but not survival

Using in-house feature extraction, my collaborators and I extracted 1605 radiomics features. This feature set was then reduced using principal component analysis (PCA). This step allowed for the reduction of the feature set independent of clinical outcomes, but still selected

features that contained the majority of the variance within the feature set. By doing so, this reduced the likelihood of overfitting the feature set to clinical outcomes, as greater than 1600 features would be represented by fewer than 30 independently selected features.

After PCA feature selection, we obtained fifteen radiomic features (**Table 7**). These features were then entered into univariate models to predict clinical outcomes. Based on the successful prediction of pathological response using volume, we believed advanced imaging features would also likely be correlated with pathologic response. To test this hypothesis, we analyzed pre-treatment CT images of locally advanced NSCLC. We first determined if radiomic features could identify tumors with gross residual disease (GRD) at the time of surgery. The fifteen selected advanced imaging features had an AUC of 0.53 to 0.66 for GRD. Seven features were significantly predictive (range AUC 0.61 to 0.66, p-value <0.05) for GRD. Two of the seven features were risk proportionate and five were inversely proportional (**Figure 6a**). We then investigated the predictive power for identifying pathologic complete response (pCR). The best performing radiomic feature, *Wavelet HLL mean*, was significantly predictive (AUC = 0.63, p-value = 0.01).

Since radiomics was able to identify both gross residual disease and pathologic complete response, I reasoned that these features would likely be significant for survival outcomes. We thus tested these features for prognostic value. However, no features were correlated to OS, LRR, or DM **(Figure 7)**.

3.3 Quantitative lymph node assessment

Given that volume, shape and textural features of primary tumors were predictive of histopathologic and clinical outcomes, I hypothesized that similar analyses of lymph nodes may add new or complementary prognostic value. I was particularly interested in understanding the pathological response not of the primary tumor, but of the lymph nodes themselves.

3.3.1 Patient selection

I identified 87 patients with distinct nodal disease. Of these, 78 patients also had CT imaging performed after the completion of chemoradiation. The average age was 60 (Range 32-75) and was predominantly Caucasian (90.4%) and female (69.9%). There was a majority of IIIA patients (83.6%) with adenocarcinoma as the predominant histology. Patient characteristics are

shown in **Table 8**. Patient outcomes are shown in **Table 9**. Median overall survival was 78 months and median LRR was not reached.

3.3.2 Quantitative imaging is unable to predict nodal downstaging

Based on my earlier work exploring the relationship between primary tumor texture and pathologic response, I was interested to determine whether lymph node volume and texture were also correlated with pathologic response. To assess this, I chose the endpoints of nodal downstaging and nodal clearance as opposed to pathologic response. Nodal downstaging occurs when patients with N2 or N3 disease at the time of staging have N1 or N0 (ypN1 or ypN0) disease at the time of surgery. Nodal clearance occurs when patients achieve N0 nodal status at the time of surgery (ypN0). These endpoints are independent of the primary tumor which is the endpoint tested by pathologic response. Nodal clearance alone however, is an important prognostic indicator for survival in patients undergoing trimodality therapy [67].

Of the patients with CT imaging available, 73 patients had N2 or N3 nodal disease. 66 patients had N2 disease at the time of presentation and 7 patients had N3 disease. All patients received concurrent chemotherapy with the majority receiving cisplatin/etoposide. 47 patients (64%) were downstaged to either ypN1 or ypN0 by pathologic staging at the time of surgery. 40 patients (54.8%) achieved nodal clearance to ypN0. Multiple imaging parameters were analyzed for correlation with nodal downstaging or clearance. Analyzing primary tumor and all involved nodal stations, the median tumor volume prior to chemoradiation was 39.1 cm^3 (Interquartile range 20.6-80.7 cm^3). The median tumor volume following chemoradiation was 19.1 cm^3 (Interquartile range 11.6-37.8 cm^3) and the mean relative change in tumor volume was -45.8% (Interquartile range -65.3 to 31.0%). There was no association with pre-treatment volume ($p=0.74$), post-treatment volume ($p=0.42$), or change in total tumor volume ($p=0.47$).

Analyzing only N2 mediastinal nodal volumes, the median N2 lymph node volume prior to chemoradiation was 6.7 cm^3 (Interquartile range 3.1-14.6 cm^3). The median N2 lymph node volume following chemoradiation was 3.8 cm^3 (Interquartile range 1.8-7.0 cm^3) and the median relative change in volume was -44.4% (Interquartile range -61.7 to -27.8%). Using logistic regression, there was no significant association between pre-treatment N2 volume ($p=0.62$), post-treatment N2 volume ($p= 0.84$), or change in volume ($p= 0.50$) and nodal downstaging. Additionally there was no significant association between pre-treatment N2 volume, post-treatment N2 volume, or change in volume and nodal clearance.

Principal component analysis of texture features identified 16 pre-treatment and 16 post-treatment images features from 1605 original features (**Table 10**). Of these, two features *Wavelet LLH stats std* and *Wavelet LLL glcm inverseVar* were identified in common between pre-treatment and post-treatment lymph node features. No features demonstrated association with either nodal clearance or nodal downstaging.

Finally, analyzing clinical features, there was no association between age, race, gender, performance status, number of positive lymph node stations, radiation dose, or clinical stage and nodal downstaging

3.3.3 Lymph node volume predicts local recurrence and overall survival

Survival outcomes of local recurrence, progression free survival and overall survival were investigated using the concordance index (c-index) and Kaplan-Meier analysis. Using the c-index, we found significant correlation between mediastinal lymph node volume and locoregional recurrence as well as overall survival (**Figure 8**). Both pre-treatment and post-treatment mediastinal lymph node volume had high c-index scores for locoregional recurrence (0.66 and 0.67 respectively) and overall survival (0.62 and 0.60 respectively). Including hilar nodal volumes in the total lymph node volume improved the c-index scores for both LRR (0.71 and 0.72 respectively) and OS (0.67 and 0.65 respectively). Notably, total tumor volume including the primary tumor at either imaging time point was not significantly associated with either local recurrence or overall survival.

Given the high c-index for lymph node volume and LRR, Kaplan Meier analysis was used to stratify patients into high-risk and low-risk groups. Patients were separated into quartile groups based on lymph node volume. Patients with mediastinal lymph node volumes greater than 14.6 cm^3, representing the upper quartile of patients, were found to have increased LRR compared to patients with lymph node volumes less than 14.6 cm^3 ($p=0.01$) (**Figure 9a**). Similarly these patients were found to have decreased OS compared to patients with lymph node volumes less than 14.6 cm^3 ($p=0.001$) (**Figure 9b**).

Additionally patients with mediastinal lymph node volume greater than 7.0 cm^3 after the completion of preoperative chemoradiation, representing the upper quartile of post-treatment volumes, were found to have increased LRR ($p<0.001$) and decreased OS ($p=0.04$) compared to patients with lymph node volume less than 7.0 cm3 volume (**Figure 9c, 9d**).

3.3.4 Lymph node texture predicts LRR, DM and OS

Due to the high predictive value for volume and survival outcomes, I reasoned that other radiomic features could also be prognostic. I then tested pre-treatment and post-treatment lymph node features for association with survival outcomes. I used the 16 pre-treatment and 16 post-treatment images features identified through PCA for this analysis. Notably, post-treatment lymph nodes had a much greater number of radiomics features associated with survival outcomes.

Analyzing pre-treatment lymph nodes, there were three quantitative features associated with LRR in addition to volume (**Figure 10a**). There were zero features associated with DM (**Figure 10b**), and one feature associated with OS (**Figure 10c**). The features associated with LRR included *Shape spherDisprop* (CI 0.72), *Stats kurtosis* (CI 0.63) and *LoG sigma 5 mm 3D glcm invDiffnorm* (CI 0.62). The feature associated with OS was *spherDisprop* (CI 0.64). The shape feature *spherical disproportionality* reflects the difference between the tumor shape and a sphere of equal volume. The *stats kurtosis* feature reflects the shape of the voxel intensity histogram. The feature *LoG sigma 5 mm 3D glcm invDiffnorm* describes the inverse difference moment (normalized) which is a measure of homogeneity within the tumor.

Post-treatment lymph node analysis revealed numerous radiomic features associated with LRR. Of the 16 features independently selected to represent the feature space, 4 features were significantly associated with local recurrence (**Figure 11a**). C-indices had a range of 0.62-0.72 for features proportional with LRR. These included a mixture of both statistics and textural based features but no shape features. The largest C-index of these features was for the *LoG sigma 4mm 3D rlgl shortRunHighGrayLevEmphasis* with a c-index of 0.72. This feature is sensitive to connecting voxels of high intensity. For DM, two features were significant from random (**Figure 11b**). These were *Wavelet HHL stats var* (CI 0.60), a measure of the variance of voxels, and *Wavelet HLL glcm contrast* (CI 0.59), correlated to textural heterogeneity. Similarly, the feature *Wavelet LLH glcm sumVar* with a C-index of 0.61 was associated with OS (**Figure 11c)**.

Based on the correlation between both pre-treatment and post-treatment imaging and clinical outcomes, I sought to determine if textural changes were associated with survival. I developed a model for the change, or delta, or radiomics features, quantified as the ratio of post-treatment features to pre-treatment features. After determining the ratio, PCA analysis was performed as previously described to select independent features. The results again demonstrated a correlation between the new delta based features and clinical outcomes. C-indices had a range

of 0.62-0.66 for features associated with LRR. The feature *LoG sigma 5 mm 3D stats entropy* had the greatest CI of the four features associated with LRR (CI 0.66). There were no features associated with DM. The feature *LoG sigma 5 mm 3D stats mean* was associated with OS (CI 0.62).

Overall these results demonstrated significant association with both volumetric, statistical, shape and textural features and the survival endpoints tested in this study.

3.4 Quantitative assessment of SBRT

Given that radiomics had significant prognostic value for patients undergoing conventional chemoradiation, I was interested in the quantitative dynamics of SBRT. This form of hypofractionated therapy is delivered over a short period of time and thus there is less time for information regarding tumor response to be obtained. Understanding the dynamics of volume change as they relate to patient outcome could thus provide a very early time point for adaptive treatment planning.

3.4.1 Patient selection

99 patients undergoing SBRT were retrospectively analyzed for quantitative tumor changes. The median age was 74 (range 46-93) with the majority of patients presenting with adenocarcinoma (46.5%) and Stage IA disease (78.8%). The median time to local recurrence was 39.2 months and the median overall survival was 28.5 months. The median endpoint of distant recurrence was not reached. Patient and treatment characteristics can be found in **Table 11** and **Table 12**.

Tumor volumes were extracted at three time points: 1) at the initiation of SBRT 2) mid point of SBRT therapy and 3) the completion of SBRT. Furthermore, I calculated the early rate of tumor shrinkage, the rate of late tumor change, as well as max and average rate changes. This resulted in a total of 10 quantitative features for analysis.

3.4.2 Volumetric changes predict survival

The median tumor size at the start of therapy was 7.26 cm^3 (range 0.59-75.41) and the median tumor at the end of therapy was 6.60 cm^3 (Range 0.27-51.65). The median relative change in tumor size -12.4% (range -54.2% to +29.2%). Analyzing all features I was unable to find any features that were correlated with LRR (**Figure 13**). However 7 out of the 10 features were significantly prognostic for any recurrence (CI 0.58-0.64). The feature, *maximum rate* was

the feature with the highest C-index at 0.64 **(Figure 14)**. This feature describes the maximal rate of volume change at any point during therapy including both early and later time points. Additionally one feature was inversely proportional to OS (**Figure 15**). Early volume change, describing the relative change in volume between the start and middle of therapy, had a c-index of 0.41 for OS.

4. Discussion

4.1 Conclusions

Quantitative imaging has the potential, along with genomic and clinical factors, to be a key component of driving personalized medicine. The goal of radiomics is to provide additional data points beyond the capabilities of the human eye. This data is particularly relevant for the treatment of cancer patients for which treatment decisions are routinely guided by imaging [68]. Radiomics can potentially offer a non-invasive method to assess changes within a malignancy that are manifest by changes in textural heterogeneity, shape or density. The aim of this project was to demonstrate a correlation between quantitative data and clinical outcomes. I tested and validated the hypothesis that data derived from clinically obtained imaging is associated with clinical outcomes and can offer additional data that complements existing clinical information.

The results of this study show several applications of quantitative imaging features. I first demonstrated that the change in tumor volume is significantly associated with pathologic correlation as well as prediction of local recurrence. This metric performed better in our patient cohort than conventional 2-dimensional cutoffs (RECIST) used in clinical practice. I extended these findings to patients with nodal disease and demonstrated that lymph node volume alone further able to stratify advanced NSCLC patients into groups with decreased rates of survival. Second, analyzing lymph nodes alone, I show that contrary to the results obtained from analyzing primary tumors, the change in lymph node volume does not predict pathological response, nor does it predict local recurrence and overall survival. I further analyzed higher order quantitative features describing tumor texture and shape. This analysis demonstrated that pre-treatment primary tumor texture predicts pathological response and that lymph node texture predicts LRR and OS. I finally attempted to apply some of these techniques to the lower quality

images obtained from cone-beam CT scans. I demonstrated that volume change using CBCT of SBRT predicts both recurrence and overall survival.

These results have potentially implications for clinical practice. For example, locally advanced NSCLC is composed of a heterogeneous tumor population but typically contains tumor that has extended to the mediastinal lymph nodes. Multiple studies have shown that mediastinal nodal clearance is a strong predictor of overall survival, suggesting that nodal tumor burden, in addition to anatomic involvement, is an important prognostic marker of survival [67,69]. These studies suggest a clear link between local disease control and overall survival. However there is controversy as to the preferred method of local therapies (radiation therapy and/or surgery). Pless et al demonstrated no significant differences in survival between chemotherapy followed by surgery versus sequential chemotherapy and RT followed by surgery [70]. Albain et al demonstrated no survival difference between concurrent chemotherapy and RT compared to concurrent chemotherapy and radiation followed by surgery [71]. Finally, Van Meerbeeck et al demonstrated that chemotherapy followed by radiotherapy has equivalent outcomes to chemotherapy followed by surgery [72]. However, such data also do not account for the variability of responses to chemoradiation, which could influence decisions regarding intensification of local therapy for select patients. Patients with a significant likelihood of achieving pCR following chemoradiation may be less likely to benefit from the addition of a second form of local therapy such as surgical resection but patients with a suboptimal response may benefit from radiation dose escalation, consolidation chemotherapy, and/or surgical resection. The results of this thesis identify volumetric and textural features that are directly correlated to tumor pathology including in the subset of stage IIIA patients. Furthermore, despite the lack of prediction for nodal clearance in our study, we establish novel cutoffs for lymph node volume that can be used to risk stratify patients with mediastinal nodal disease.

To our knowledge this is the first study identifying prognostic quantitative imaging features in neoadjuvant chemoradiation. Prior work in quantitative imaging has primarily been limited to non-surgical cases and predominately analyzing one imaging time point [22,23]. These studies describe an association with tumor volume and survival that we did not find in our study. Koo et al further investigated changes in tumor volume but did not find an association between tumor volume change and survival [63]. Our results contrast those findings, in that volumetric changes was associated with LRR when limited to locally advanced stage IIIA patients. We

further describe the size and texture relationship for pathologic response that more accurately describe radiopathologic correlation. Texture features were unable to predict survival, similar to a previous study from Ravanelli et al. [27].

A few results have contradictory findings compared to prior literature. We report that both pre-treatment and post-treatment lymph node volume during neoadjuvant therapy were significantly associated with survival. However Dehing-Oberije et al and Basaki et al previously reported no association between nodal volume and survival [25,74]. Such differences may be partially explained by heterogeneity in treatment modalities, tumor volume thresholds and segmentation used in these studies.

The novel lymph node features are the multiple texture features correlated to local recurrence, distant metastasis and overall survival. To our knowledge, no lymph node features have been identified in a cohort as large as ours. Although we were unable to develop a multivariate textural signature, we were able to generate multiple features that were associated with clinical endpoints in both pre-treatment and post-treatment lymph nodes. Additionally, this study demonstrated the use of delta radiomics, as a means of providing information about the response to therapy. These results could be extrapolated to additional time points to be used for more accurate and frequent non-invasive monitoring of tumor response. Although the CI of these was below 0.80 for all features investigated, these features provide a foundation for further investigation before use as imaging biomarkers.

Overall these results agree with prior radiomics findings that find association between clinical outcomes and quantitative imaging [46,60,68]

4.2 Limitations of the study

There are many challenges and limitation that are concerning for the field of quantitative imaging and radiomics. With respect to this study, the retrospective nature of these analyses at our single institution limit the generalizability of this data. The small sample size and low incidence of pCR in this study resulted in insufficient power to build multivariate models and will require further validation in larger cohorts. I also recognize that patients in this study are composed of heterogeneous stages which may further affect the generalizability of the study. However, we also find that our results hold true for all patients with operable locally advanced patients as well as only the stage IIIA patients in subgroup analysis.

With respect to the limitation of the field, these can be generally grouped into 1) acquisition and reproducibility of data and 2) the clinical utility of the data obtained. Image acquisition remains a challenge for radiomics analysis due to the variability in image acquisition across instruments and institutions [75]. Image acquisition is often not standardized with respect to image slice thickness, reconstruction algorithms, and image resolution. Such imaging variability affects the development of imaging databases [47]. Such features are more difficult to reproduce in PET or MRI images. PET and MRI are particularly challenging due to variations in institutional protocols including dose uptake, metabolic volume reconstruction, and motion susceptibility. Despite these challenges, there is evidence demonstrating the robustness of radiomics features. Radiomics features are stable with respect to sequential CT images obtained 15 minutes apart [76,77] and repeated PET imaging [78]. At the very least, these studies demonstrate radiomic stability at the institutional level which provides support for the data in our study. Additional studies of variability remain challenging, such as noise introduced as a result respiratory motion [79]. Another problem with radiomics acquisition is the variability of segmentation. Automated segmentation may help address some of these issues as features derived from automated contours yield more reproducible results than manual contours [80]. Furthermore, based on the hypothesis that the central component of the tumor is most consistent across segmentation, radiomics features remain robust within the central core of the tumor. This then avoids the limitations of segmentation due to noise from differential contours [81].

It is unclear whether the tumor phenotype obtained from radiomics corresponds to an underlying biological genotype. The textural features in this study indicated that patients with increased heterogeneity of texture are more likely to have more aggressive disease. Yet it remains to be determined what the actual biological significance of textural or statistical features is. However, there is some evidence that indicates a the correlation between biological phenotype and imaging phenotype. Xenograft models in mice have demonstrated that radiomics features change significantly during expression of the inducible GADD34 [82]. Furthermore, radiomics features have been correlated to ALK and ROS1 [83], triple negative breast cancer on MRI [84,85], as well as histopathology [58,86]. Work from our laboratory (unpublished) has also identified radiomics features that are correlated with EGFR and KRAS mutation status, further adding support to the idea that radiomics features reflect biological features.

4.3 Future directions

4.3.1 Delta radiomics

In many prior quantitative imaging studies radiomic features are limited to features extracted at a single single time point imaging. However, based on the predictive capability of changes in volume, I believe there is a significant amount of information that can likely be gained be observed changes in radiomic features as well. Currently my collaborators and I are working to build models of radiomics that can incorporate the *delta* of radiomics data including those presented in this study. The data presented in this work regarding the change in texture over the course of two CT imaging time points is particularly exciting as there have yet to be any studies regarding serial changes in texture over the course of chemoradiation. Furthermore, as more patients receive novel therapies, the applications of quantitative imaging will also grow. Imaging for surveillance could not only assess response, but could be used in active surveillance to determine the development of resistance before it is clinically apparent.

4.3.2 CBCT radiomics and adaptive treatment planning

CBCTs are a lower quality CT image obtained at the time of SBRT treatment for ensuring radiation is delivered to the same area during each fraction. The initial data presented in this study demonstrated that volume changes on CBCT are correlated with clinical outcomes. Although it is known that volume changes occur during SBRT therapy [87], it is unclear how much information regarding tumor response can be gained from volume alone. Despite the limitations of time, I was able to demonstrate that volumetric changes during SBRT treatment can be correlated with survival. Based on the data presented in this work, it is very likely that higher order features will offer additional information [42]. This is based on the hypothesis that texture features will change more rapidly than volume.

As a result of building models that incorporated CBCT texture, we hope to be able to develop protocols for adaptive treatment planning. Although challenges to this have already been described above, a major goal of quantitative imaging is to be able to assess the efficacy of treatments in progress and modify them accordingly. Such modifications could include modifying tumor segmentation, dose escalation and/or decisions regarding surgical resection.

4.4 Summary

In this work, I sought to apply the principles of quantitative imaging to NSCLC lung cancer patients. This study demonstrated application of all aspects of radiomics including volume, shape, statistics and texture to NSCLC patients. These quantitative imaging features were applied to novel clinical scenarios including patients undergoing neoadjuvant therapy, lymph node analysis, and the low-resolution CBCT images. I not only demonstrated the novel correlation with pathologic response, but found several features prognostic for overall survival, progression-free survival, and locoregional recurrence-free survival. These examples highlight the potential within the rapidly growing field of quantitative imaging to more robustly describe tumor phenotype than conventional imaging criteria. These results provide novel evidence to the growing radiomics literature that there is significant association between imaging, pathology and clinical outcomes. Further exploration will allow for more complete models describing tumor imaging phenotype with clinical outcomes.

Author contributions

All work presented in this thesis was performed by Vishesh Agrawal under the supervision and guidance of Dr. Raymond Mak and Dr. Hugo Aerts.

A detailed description of all work involved in the data gathering, generation, and analysis for this project is listed below.

Project Component	**Contributions**
Project design and development	Vishesh Agrawal with Principal Investigators Dr. Raymond Mak and Dr. Hugo Aerts
Patient identification and database annotation	1) Clinical patient database developed and curated by Dr. Raymond Mak with assistance from Stephanie Lee and John Romano 2) Patient identification and database annotation for quantitative imaging performed by Vishesh Agrawal
Tumor Segmentation (supervised by RHM)	1) Vishesh Agrawal segmented the majority of cases in section 3.1 with assistance from Thibaud Coroller and Ying Hou 2) Vishesh Agrawal and Thibaud Coroller contributed equally to the segmentation of cases in results section 3.2 3) Vishesh Agrawal segmented the entirety of cases in results section 3.3 4) Ying Hou segmented the majority of cases in results section 3.4 with assistance from Vishesh Agrawal
Radiomics feature extraction from CT images	1) In-house Radiomics software and platform previously developed by Principal Investigator Dr. Hugo Aerts (see citation [46]). 2) Vivek Narayan performed export of images to 3D slicer software, extraction of radiomics features and data export.
Data analysis	1) Vishesh Agrawal performed all data analysis for results section 3.1 2) Vishesh Agrawal contributed partially to data analysis in results section 3.2 with Thibaud Coroller contributing to majority of data analysis 3) Vishesh Agrawal performed all data analysis for results in section 3.3 with assistance from Thibaud Coroller 4) Vishesh Agrawal performed all data analysis for results in section 3.4

References

[1] Lozano R, Naghavi M, Foreman K, Lim S, Shibuya K, Aboyans V, et al. Global and regional mortality from 235 causes of death for 20 age groups in 1990 and 2010: a systematic analysis for the Global Burden of Disease Study 2010. The Lancet 2012;380:2095–128. doi:10.1016/S0140-6736(12)61728-0.

[2] Ettinger DS, Akerley W, Borghaei H, Chang AC, Cheney RT, Chirieac LR, et al. Non-small cell lung cancer, version 2.2013. J Natl Compr Cancer Netw JNCCN 2013;11:645–53; quiz 653.

[3] Molina JR, Yang P, Cassivi SD, Schild SE, Adjei AA. Non–Small Cell Lung Cancer: Epidemiology, Risk Factors, Treatment, and Survivorship. Mayo Clin Proc Mayo Clin 2008;83:584–94.

[4] Chen Z, Fillmore CM, Hammerman PS, Kim CF, Wong K-K. Non-small-cell lung cancers: a heterogeneous set of diseases. Nat Rev Cancer 2014;14:535–46. doi:10.1038/nrc3775.

[5] Ko YC, Lee CH, Chen MJ, Huang CC, Chang WY, Lin HJ, et al. Risk factors for primary lung cancer among non-smoking women in Taiwan. Int J Epidemiol 1997;26:24–31.

[6] Reck M, Heigener DF, Mok T, Soria J-C, Rabe KF. Management of non-small-cell lung cancer: recent developments. Lancet Lond Engl 2013;382:709–19. doi:10.1016/S0140-6736(13)61502-0.

[7] Johnson DH, Schiller JH, Bunn PA. Recent Clinical Advances in Lung Cancer Management. J Clin Oncol 2014;32:973–82. doi:10.1200/JCO.2013.53.1228.

[8] Morales-Espinosa D, García-Román S, Teixidó C, Karachaliou N, Rosell R. Immunotherapy meets targeted therapy: will this team end the war against cancer? Transl Lung Cancer Res 2015;4:752–5. doi:10.3978/j.issn.2218-6751.2015.12.05.

[9] Medina PJ, Adams VR. PD-1 Pathway Inhibitors: Immuno-Oncology Agents for Restoring Antitumor Immune Responses. Pharmacotherapy 2016. doi:10.1002/phar.1714.

[10] Korpanty GJ, Graham DM, Vincent MD, Leighl NB. Biomarkers That Currently Affect Clinical Practice in Lung Cancer: EGFR, ALK, MET, ROS-1, and KRAS. Front Oncol 2014;4. doi:10.3389/fonc.2014.00204.

[11] Huncharek M, Muscat J, Geschwind JF. K-ras oncogene mutation as a prognostic marker in non-small cell lung cancer: a combined analysis of 881 cases. Carcinogenesis 1999;20:1507–10.

[12] Carter CA, Rajan A, Keen C, Szabo E, Khozin S, Thomas A, et al. Selumetinib with and without erlotinib in KRAS mutant and KRAS wild-type advanced non-small cell lung cancer. Ann Oncol Off J Eur Soc Med Oncol ESMO 2016. doi:10.1093/annonc/mdw008.

[13] Huncharek M, Kupelnick B, Geschwind JF, Caubet JF. Prognostic significance of p53 mutations in non-small cell lung cancer: a meta-analysis of 829 cases from eight published studies. Cancer Lett 2000;153:219–26.

[14] Doebele RC, Pilling AB, Aisner DL, Kutateladze TG, Le AT, Weickhardt AJ, et al. Mechanisms of resistance to crizotinib in patients with ALK gene rearranged non-small cell lung cancer. Clin Cancer Res Off J Am Assoc Cancer Res 2012;18:1472–82. doi:10.1158/1078-0432.CCR-11-2906.

[15] Awad MM, Katayama R, McTigue M, Liu W, Deng Y-L, Brooun A, et al. Acquired resistance to crizotinib from a mutation in CD74-ROS1. N Engl J Med 2013;368:2395–401. doi:10.1056/NEJMoa1215530.
[16] Taenzer A, Alix-Panabières C, Wikman H, Pantel K. Circulating tumor-derived biomarkers in lung cancer. J Thorac Dis 2012;4:448–9. doi:10.3978/j.issn.2072-1439.2012.08.17.
[17] Wong MP. Circulating tumor cells as lung cancer biomarkers. J Thorac Dis 2012;4:631–4. doi:10.3978/j.issn.2072-1439.2012.10.05.
[18] Hennessey PT, Sanford T, Choudhary A, Mydlarz WW, Brown D, Adai AT, et al. Serum microRNA biomarkers for detection of non-small cell lung cancer. PloS One 2012;7:e32307. doi:10.1371/journal.pone.0032307.
[19] Therasse P, Arbuck SG, Eisenhauer EA, Wanders J, Kaplan RS, Rubinstein L, et al. New guidelines to evaluate the response to treatment in solid tumors. European Organization for Research and Treatment of Cancer, National Cancer Institute of the United States, National Cancer Institute of Canada. J Natl Cancer Inst 2000;92:205–16.
[20] Eisenhauer EA, Therasse P, Bogaerts J, Schwartz LH, Sargent D, Ford R, et al. New response evaluation criteria in solid tumours: revised RECIST guideline (version 1.1). Eur J Cancer Oxf Engl 1990 2009;45:228–47. doi:10.1016/j.ejca.2008.10.026.
[21] Tuma RS. Sometimes Size Doesn't Matter: Reevaluating RECIST and Tumor Response Rate Endpoints. J Natl Cancer Inst 2006;98:1272–4. doi:10.1093/jnci/djj403.
[22] Bradley JD, Ieumwananonthachai N, Purdy JA, Wasserman TH, Lockett MA, Graham MV, et al. Gross tumor volume, critical prognostic factor in patients treated with three-dimensional conformal radiation therapy for non-small-cell lung carcinoma. Int J Radiat Oncol Biol Phys 2002;52:49–57.
[23] Alexander BM, Othus M, Caglar HB, Allen AM. Tumor volume is a prognostic factor in non-small-cell lung cancer treated with chemoradiotherapy. Int J Radiat Oncol Biol Phys 2011;79:1381–7. doi:10.1016/j.ijrobp.2009.12.060.
[24] Bahce I, Vos CG, Dickhoff C, Hartemink KJ, Dahele M, Smit EF, et al. Metabolic activity measured by FDG PET predicts pathological response in locally advanced superior sulcus NSCLC. Lung Cancer Amst Neth 2014;85:205–12. doi:10.1016/j.lungcan.2014.04.010.
[25] Dehing-Oberije C, De Ruysscher D, van der Weide H, Hochstenbag M, Bootsma G, Geraedts W, et al. Tumor volume combined with number of positive lymph node stations is a more important prognostic factor than TNM stage for survival of non-small-cell lung cancer patients treated with (chemo)radiotherapy. Int J Radiat Oncol Biol Phys 2008;70:1039–44. doi:10.1016/j.ijrobp.2007.07.2323.
[26] Stinchcombe TE, Morris DE, Moore DT, Bechtel JH, Halle JS, Mears A, et al. Post-chemotherapy gross tumor volume is predictive of survival in patients with stage III non-small cell lung cancer treated with combined modality therapy. Lung Cancer Amst Neth 2006;52:67–74. doi:10.1016/j.lungcan.2005.11.008.
[27] Ravanelli M, Farina D, Morassi M, Roca E, Cavalleri G, Tassi G, et al. Texture analysis of advanced non-small cell lung cancer (NSCLC) on contrast-enhanced computed tomography: prediction of the response to the first-line chemotherapy. Eur Radiol 2013;23:3450–5. doi:10.1007/s00330-013-2965-0.
[28] Reymen B, Van Loon J, van Baardwijk A, Wanders R, Borger J, Dingemans A-MC, et al. Total gross tumor volume is an independent prognostic factor in patients treated with

selective nodal irradiation for stage I to III small cell lung cancer. Int J Radiat Oncol Biol Phys 2013;85:1319–24. doi:10.1016/j.ijrobp.2012.10.003.
[29] William WN, Pataer A, Kalhor N, Correa AM, Rice DC, Wistuba II, et al. Computed tomography RECIST assessment of histopathologic response and prediction of survival in patients with resectable non-small-cell lung cancer after neoadjuvant chemotherapy. J Thorac Oncol Off Publ Int Assoc Study Lung Cancer 2013;8:222–8. doi:10.1097/JTO.0b013e3182774108.
[30] Pataer A, Kalhor N, Correa AM, Raso MG, Erasmus JJ, Kim ES, et al. Histopathologic response criteria predict survival of patients with resected lung cancer after neoadjuvant chemotherapy. J Thorac Oncol Off Publ Int Assoc Study Lung Cancer 2012;7:825–32. doi:10.1097/JTO.0b013e318247504a.
[31] Yamane Y, Ishii G, Goto K, Kojima M, Nakao M, Shimada Y, et al. A novel histopathological evaluation method predicting the outcome of non-small cell lung cancer treated by neoadjuvant therapy: the prognostic importance of the area of residual tumor. J Thorac Oncol Off Publ Int Assoc Study Lung Cancer 2010;5:49–55. doi:10.1097/JTO.0b013e3181c0a1f8.
[32] Pisters KM, Kris MG, Gralla RJ, Zaman MB, Heelan RT, Martini N. Pathologic complete response in advanced non-small-cell lung cancer following preoperative chemotherapy: implications for the design of future non-small-cell lung cancer combined modality trials. J Clin Oncol Off J Am Soc Clin Oncol 1993;11:1757–62.
[33] Mouillet G, Monnet E, Milleron B, Puyraveau M, Quoix E, David P, et al. Pathologic complete response to preoperative chemotherapy predicts cure in early-stage non-small-cell lung cancer: combined analysis of two IFCT randomized trials. J Thorac Oncol Off Publ Int Assoc Study Lung Cancer 2012;7:841–9. doi:10.1097/JTO.0b013e31824c7d92.
[34] Isobe K, Hata Y, Sakaguchi S, Sato F, Takahashi S, Sato K, et al. Pathological response and prognosis of stage III non-small cell lung cancer patients treated with induction chemoradiation. Asia Pac J Clin Oncol 2012;8:260–6. doi:10.1111/j.1743-7563.2012.01529.x.
[35] Ricardi U, Badellino S, Filippi AR. Stereotactic body radiotherapy for early stage lung cancer: History and updated role. Lung Cancer Amst Neth 2015;90:388–96. doi:10.1016/j.lungcan.2015.10.016.
[36] Sroufe R, Kong F-MS. Triaging early-stage lung cancer patients into non-surgical pathways: who, when, and what? Transl Lung Cancer Res 2015;4:438–47. doi:10.3978/j.issn.2218-6751.2015.07.22.
[37] Simone CB, Dorsey JF. Additional data in the debate on stage I non-small cell lung cancer: surgery versus stereotactic ablative radiotherapy. Ann Transl Med 2015;3:172. doi:10.3978/j.issn.2305-5839.2015.07.26.
[38] Chang JY, Senan S, Paul MA, Mehran RJ, Louie AV, Balter P, et al. Stereotactic ablative radiotherapy versus lobectomy for operable stage I non-small-cell lung cancer: a pooled analysis of two randomised trials. Lancet Oncol 2015;16:630–7. doi:10.1016/S1470-2045(15)70168-3.
[39] Kress M-AS, Collins BT, Collins SP, Dritschilo A, Gagnon G, Unger K. Scoring system predictive of survival for patients undergoing stereotactic body radiation therapy for liver tumors. Radiat Oncol Lond Engl 2012;7:148. doi:10.1186/1748-717X-7-148.

[40] Bortolin MT, Tedeschi R, Bidoli E, Furlan C, Basaglia G, Minatel E, et al. Cell-free DNA as a prognostic marker in stage I non-small-cell lung cancer patients undergoing stereotactic body radiotherapy. Biomark Biochem Indic Expo Response Susceptibility Chem 2015;20:422–8. doi:10.3109/1354750X.2015.1094139.
[41] Matsuo Y, Shibuya K, Nagata Y, Takayama K, Norihisa Y, Mizowaki T, et al. Prognostic factors in stereotactic body radiotherapy for non-small-cell lung cancer. Int J Radiat Oncol Biol Phys 2011;79:1104–11. doi:10.1016/j.ijrobp.2009.12.022.
[42] Fave X, Mackin D, Yang J, Zhang J, Fried D, Balter P, et al. Can radiomics features be reproducibly measured from CBCT images for patients with non-small cell lung cancer? Med Phys 2015;42:6784. doi:10.1118/1.4934826.
[43] Wang H, Schabath MB, Liu Y, Berglund AE, Bloom GC, Kim J, et al. Semiquantitative Computed Tomography Characteristics for Lung Adenocarcinoma and Their Association With Lung Cancer Survival. Clin Lung Cancer 2015;16:e141–63. doi:10.1016/j.cllc.2015.05.007.
[44] Velazquez ER, Parmar C, Jermoumi M, Mak RH, van Baardwijk A, Fennessy FM, et al. Volumetric CT-based segmentation of NSCLC using 3D-Slicer. Sci Rep 2013;3:3529. doi:10.1038/srep03529.
[45] Lambin P, Rios-Velazquez E, Leijenaar R, Carvalho S, van Stiphout RGPM, Granton P, et al. Radiomics: extracting more information from medical images using advanced feature analysis. Eur J Cancer Oxf Engl 1990 2012;48:441–6. doi:10.1016/j.ejca.2011.11.036.
[46] Aerts HJWL, Velazquez ER, Leijenaar RTH, Parmar C, Grossmann P, Carvalho S, et al. Decoding tumour phenotype by noninvasive imaging using a quantitative radiomics approach. Nat Commun 2014;5:4006. doi:10.1038/ncomms5006.
[47] Kumar V, Gu Y, Basu S, Berglund A, Eschrich SA, Schabath MB, et al. Radiomics: the process and the challenges. Magn Reson Imaging 2012;30:1234–48. doi:10.1016/j.mri.2012.06.010.
[48] Gunn SR. On the discrete representation of the Laplacian of Gaussian. Pattern Recognit 1999;32:1463–72. doi:10.1016/S0031-3203(98)00163-0.
[49] Sharifi M, Fathy M, Tayefeh Mahmoudi M. A classified and comparative study of edge detection algorithms. Int. Conf. Inf. Technol. Coding Comput. 2002 Proc., 2002, p. 117–20. doi:10.1109/ITCC.2002.1000371.
[50] Ypsilantis P-P, Siddique M, Sohn H-M, Davies A, Cook G, Goh V, et al. Predicting Response to Neoadjuvant Chemotherapy with PET Imaging Using Convolutional Neural Networks. PloS One 2015;10:e0137036. doi:10.1371/journal.pone.0137036.
[51] Ha S, Choi H, Cheon GJ, Kang KW, Chung J-K, Kim EE, et al. Autoclustering of Non-small Cell Lung Carcinoma Subtypes on (18)F-FDG PET Using Texture Analysis: A Preliminary Result. Nucl Med Mol Imaging 2014;48:278–86. doi:10.1007/s13139-014-0283-3.
[52] Diehn M, Nardini C, Wang DS, McGovern S, Jayaraman M, Liang Y, et al. Identification of noninvasive imaging surrogates for brain tumor gene-expression modules. Proc Natl Acad Sci U S A 2008;105:5213–8. doi:10.1073/pnas.0801279105.
[53] Vallières M, Freeman CR, Skamene SR, El Naqa I. A radiomics model from joint FDG-PET and MRI texture features for the prediction of lung metastases in soft-tissue sarcomas of the extremities. Phys Med Biol 2015;60:5471–96. doi:10.1088/0031-9155/60/14/5471.

[54] Gillies RJ, Kinahan PE, Hricak H. Radiomics: Images Are More than Pictures, They Are Data. Radiology 2015:151169. doi:10.1148/radiol.2015151169.
[55] Andersen MB, Harders SW, Ganeshan B, Thygesen J, Torp Madsen HH, Rasmussen F. CT texture analysis can help differentiate between malignant and benign lymph nodes in the mediastinum in patients suspected for lung cancer. Acta Radiol Stockh Swed 1987 2015. doi:10.1177/0284185115598808.
[56] Wibmer A, Hricak H, Gondo T, Matsumoto K, Veeraraghavan H, Fehr D, et al. Haralick texture analysis of prostate MRI: utility for differentiating non-cancerous prostate from prostate cancer and differentiating prostate cancers with different Gleason scores. Eur Radiol 2015;25:2840–50. doi:10.1007/s00330-015-3701-8.
[57] Cameron A, Khalvati F, Haider M, Wong A. MAPS: A Quantitative Radiomics Approach for Prostate Cancer Detection. IEEE Trans Biomed Eng 2015. doi:10.1109/TBME.2015.2485779.
[58] Lubner MG, Stabo N, Lubner SJ, Del Rio AM, Song C, Halberg RB, et al. CT textural analysis of hepatic metastatic colorectal cancer: pre-treatment tumor heterogeneity correlates with pathology and clinical outcomes. Abdom Imaging 2015;40:2331–7. doi:10.1007/s00261-015-0438-4.
[59] Cunliffe A, Armato SG, Castillo R, Pham N, Guerrero T, Al-Hallaq HA. Lung texture in serial thoracic computed tomography scans: correlation of radiomics-based features with radiation therapy dose and radiation pneumonitis development. Int J Radiat Oncol Biol Phys 2015;91:1048–56. doi:10.1016/j.ijrobp.2014.11.030.
[60] Coroller TP, Grossmann P, Hou Y, Rios Velazquez E, Leijenaar RTH, Hermann G, et al. CT-based radiomic signature predicts distant metastasis in lung adenocarcinoma. Radiother Oncol J Eur Soc Ther Radiol Oncol 2015;114:345–50. doi:10.1016/j.radonc.2015.02.015.
[61] Cook GJR, O'Brien ME, Siddique M, Chicklore S, Loi HY, Sharma B, et al. Non-Small Cell Lung Cancer Treated with Erlotinib: Heterogeneity of (18)F-FDG Uptake at PET-Association with Treatment Response and Prognosis. Radiology 2015;276:883–93. doi:10.1148/radiol.2015141309.
[62] Pieper S, Halle M, Kikinis R. 3D SLICER. Proc 1st IEEE Int Symp Biomed Imaging Nano Macro 2004:632–5.
[63] Koo TR, Moon SH, Lim YJ, Kim JY, Kim Y, Kim TH, et al. The effect of tumor volume and its change on survival in stage III non-small cell lung cancer treated with definitive concurrent chemoradiotherapy. Radiat Oncol Lond Engl 2014;9:283. doi:10.1186/s13014-014-0283-6.
[64] DeLong ER, DeLong DM, Clarke-Pearson DL. Comparing the areas under two or more correlated receiver operating characteristic curves: a nonparametric approach. Biometrics 1988;44:837–45.
[65] Ruopp MD, Perkins NJ, Whitcomb BW, Schisterman EF. Youden Index and optimal cut-point estimated from observations affected by a lower limit of detection. Biom J Biom Z 2008;50:419–30. doi:10.1002/bimj.200710415.
[66] Fine JP, Gray RJ. A Proportional Hazards Model for the Subdistribution of a Competing Risk. J Am Stat Assoc 1999;94:496–509. doi:10.1080/01621459.1999.10474144.
[67] Suntharalingam M, Paulus R, Edelman MJ, Krasna M, Burrows W, Gore E, et al. Radiation therapy oncology group protocol 02-29: a phase II trial of neoadjuvant

therapy with concurrent chemotherapy and full-dose radiation therapy followed by surgical resection and consolidative therapy for locally advanced non-small cell carcinoma of the lung. Int J Radiat Oncol Biol Phys 2012;84:456–63. doi:10.1016/j.ijrobp.2011.11.069.
[68] Lambin P, Zindler J, Vanneste B, De Voorde LV, Eekers D, Compter I, et al. Decision support systems for personalized and participative radiation oncology. Adv Drug Deliv Rev 2016. doi:10.1016/j.addr.2016.01.006.
[69] Bueno R, Richards WG, Swanson SJ, Jaklitsch MT, Lukanich JM, Mentzer SJ, et al. Nodal stage after induction therapy for stage IIIA lung cancer determines patient survival. Ann Thorac Surg 2000;70:1826–31.
[70] Pless M, Stupp R, Ris H-B, Stahel RA, Weder W, Thierstein S, et al. Induction chemoradiation in stage IIIA/N2 non-small-cell lung cancer: a phase 3 randomised trial. Lancet Lond Engl 2015;386:1049–56. doi:10.1016/S0140-6736(15)60294-X.
[71] Albain KS, Swann RS, Rusch VW, Turrisi AT, Shepherd FA, Smith C, et al. Radiotherapy plus chemotherapy with or without surgical resection for stage III non-small-cell lung cancer: a phase III randomised controlled trial. Lancet 2009;374:379–86. doi:10.1016/S0140-6736(09)60737-6.
[72] van Meerbeeck JP, Kramer GWPM, Van Schil PEY, Legrand C, Smit EF, Schramel F, et al. Randomized controlled trial of resection versus radiotherapy after induction chemotherapy in stage IIIA-N2 non-small-cell lung cancer. J Natl Cancer Inst 2007;99:442–50. doi:10.1093/jnci/djk093.
[73] Vokes EE, Herndon JE, Kelley MJ, Cicchetti MG, Ramnath N, Neill H, et al. Induction chemotherapy followed by chemoradiotherapy compared with chemoradiotherapy alone for regionally advanced unresectable stage III Non-small-cell lung cancer: Cancer and Leukemia Group B. J Clin Oncol Off J Am Soc Clin Oncol 2007;25:1698–704. doi:10.1200/JCO.2006.07.3569.
[74] Basaki K, Abe Y, Aoki M, Kondo H, Hatayama Y, Nakaji S. Prognostic factors for survival in stage III non-small-cell lung cancer treated with definitive radiation therapy: impact of tumor volume. Int J Radiat Oncol Biol Phys 2006;64:449–54. doi:10.1016/j.ijrobp.2005.07.967.
[75] Mackin D, Fave X, Zhang L, Fried D, Yang J, Taylor B, et al. Measuring Computed Tomography Scanner Variability of Radiomics Features. Invest Radiol 2015;50:757–65. doi:10.1097/RLI.0000000000000180.
[76] Balagurunathan Y, Gu Y, Wang H, Kumar V, Grove O, Hawkins S, et al. Reproducibility and Prognosis of Quantitative Features Extracted from CT Images. Transl Oncol 2014;7:72–87.
[77] Balagurunathan Y, Kumar V, Gu Y, Kim J, Wang H, Liu Y, et al. Test-retest reproducibility analysis of lung CT image features. J Digit Imaging 2014;27:805–23. doi:10.1007/s10278-014-9716-x.
[78] Leijenaar RTH, Carvalho S, Velazquez ER, van Elmpt WJC, Parmar C, Hoekstra OS, et al. Stability of FDG-PET Radiomics features: an integrated analysis of test-retest and inter-observer variability. Acta Oncol Stockh Swed 2013;52:1391–7. doi:10.3109/0284186X.2013.812798.
[79] Oliver JA, Budzevich M, Zhang GG, Dilling TJ, Latifi K, Moros EG. Variability of Image Features Computed from Conventional and Respiratory-Gated PET/CT Images of Lung Cancer. Transl Oncol 2015;8:524–34. doi:10.1016/j.tranon.2015.11.013.

[80] Parmar C, Rios Velazquez E, Leijenaar R, Jermoumi M, Carvalho S, Mak RH, et al. Robust Radiomics feature quantification using semiautomatic volumetric segmentation. PloS One 2014;9:e102107. doi:10.1371/journal.pone.0102107.
[81] Echegaray S, Gevaert O, Shah R, Kamaya A, Louie J, Kothary N, et al. Core samples for radiomics features that are insensitive to tumor segmentation: method and pilot study using CT images of hepatocellular carcinoma. J Med Imaging Bellingham Wash 2015;2:041011. doi:10.1117/1.JMI.2.4.041011.
[82] Panth KM, Leijenaar RTH, Carvalho S, Lieuwes NG, Yaromina A, Dubois L, et al. Is there a causal relationship between genetic changes and radiomics-based image features? An in vivo preclinical experiment with doxycycline inducible GADD34 tumor cells. Radiother Oncol J Eur Soc Ther Radiol Oncol 2015;116:462–6. doi:10.1016/j.radonc.2015.06.013.
[83] Yoon HJ, Sohn I, Cho JH, Lee HY, Kim J-H, Choi Y-L, et al. Decoding Tumor Phenotypes for ALK, ROS1, and RET Fusions in Lung Adenocarcinoma Using a Radiomics Approach. Medicine (Baltimore) 2015;94:e1753. doi:10.1097/MD.0000000000001753.
[84] Zhu Y, Li H, Guo W, Drukker K, Lan L, Giger ML, et al. Deciphering Genomic Underpinnings of Quantitative MRI-based Radiomic Phenotypes of Invasive Breast Carcinoma. Sci Rep 2015;5:17787. doi:10.1038/srep17787.
[85] Wang J, Kato F, Oyama-Manabe N, Li R, Cui Y, Tha KK, et al. Identifying Triple-Negative Breast Cancer Using Background Parenchymal Enhancement Heterogeneity on Dynamic Contrast-Enhanced MRI: A Pilot Radiomics Study. PloS One 2015;10:e0143308. doi:10.1371/journal.pone.0143308.
[86] Ganeshan B, Goh V, Mandeville HC, Ng QS, Hoskin PJ, Miles KA. Non-small cell lung cancer: histopathologic correlates for texture parameters at CT. Radiology 2013;266:326–36. doi:10.1148/radiol.12112428.
[87] Bhatt AD, El-Ghamry MN, Dunlap NE, Bhatt G, Harkenrider MM, Schuler JC, et al. Tumor volume change with stereotactic body radiotherapy (SBRT) for early-stage lung cancer: evaluating the potential for adaptive SBRT. Am J Clin Oncol 2015;38:41–6. doi:10.1097/COC.0b013e318287bd7f.

Tables and Figures

Figure 1: Radiomics methods overview. CT images are segmented manually in treatment planning software such as MIM or Eclipse (A). Images are then exported to 3D-slicer software where the region of interest is isolated and resampled in 3 mm x 3mm x 3mm voxels (B). Images are then analyzed for shape, statistics and texture features. Wavelet or Laplacian of Gaussian (LoG) filters are applied resulting in a set of 1605 unique features (C). The radiomics data is subsequently analyzed for association with clinical outcomes. Abbreviations: RLGL= run length gray level, GLCM=gray level co-occurrence matrix, GLSZM=gray level size zone matrix, LoG=Laplacian of Gaussian
Adapted from Aerts et al, 2014, and Coroller et al, 2015.

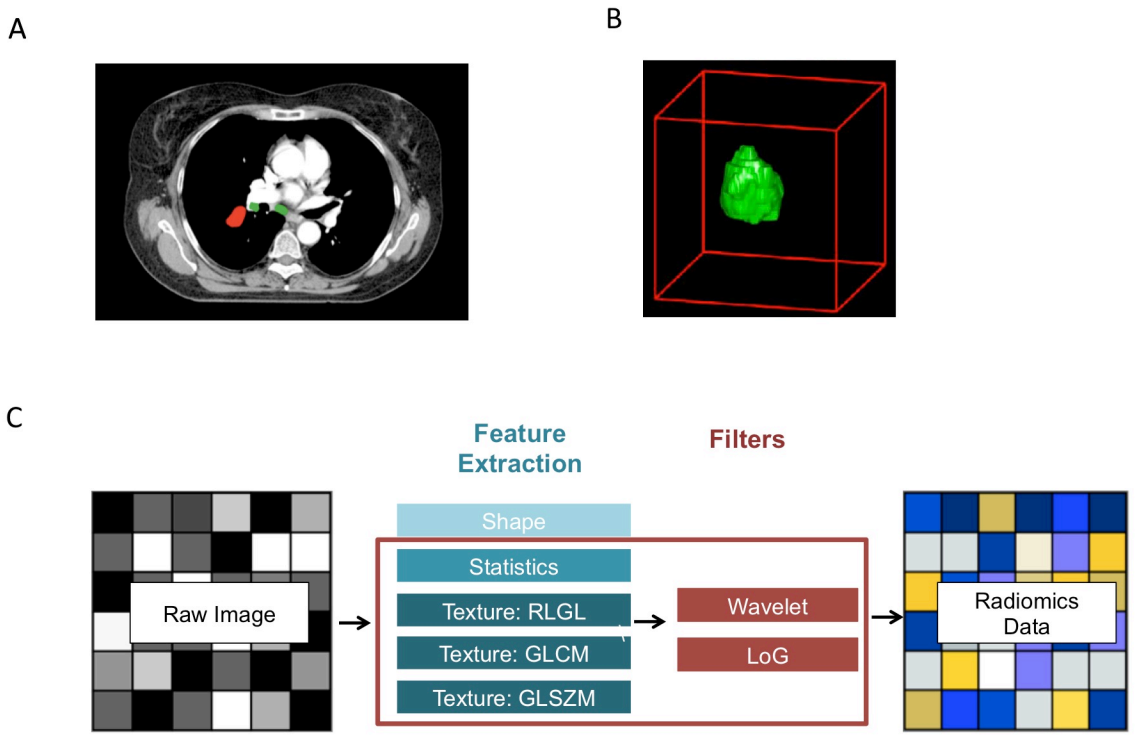

Figure 2: Computation of textural features performed using gray level co-occurrence matrices (GLCM). GLCM matrices describes the relationship between intensity levels occurring in two pixels within the image. In the GLCM matrix P(i,j,δ,α), the (i,j)th element represents the number of times the combination of intensity levels i and j occur in two pixels in the image I. δ represents the number of pixels separating i and j in the direction α. For example, a two-dimensional image I with 5 discrete gray levels can be resampled into discrete pixels (A). Within image I, the gray levels 1 and 2 are separated by one pixel in the horizontal direction three times (B). The GLCM matrix P, in which $\delta=1$ and α represents the horizontal 0 degrees (C). In this matrix (i,j)=(1,2) takes the value of 3. This process is then applied throughout the 3-dimensional tumor (D). Additional texture matrices Run-Length Gray-Level (RLGL) and Gray Level Size Zone (GLSZM) are not shown here. GLSZM and RLGL matrices are similar to GLCM matrices but represent the number of occurrences of pixels of the same intensity connected in sequence.
Adapted from Aerts et al, 2014.

A

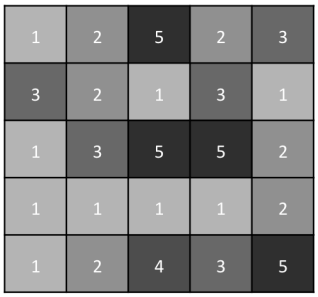

B

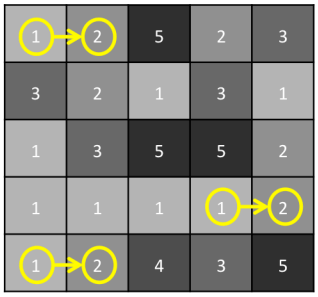

C

i \ j	1	2	3	4	5
1	3	3	2	0	0
2	1	0	1	1	1
3	1	1	0	0	2
4	0	0	1	0	0
5	0	2	0	0	1

D

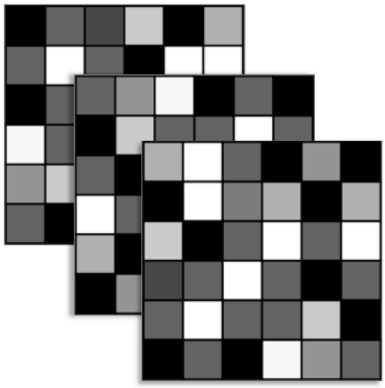

Table 1: Descriptions of selected radiomics features
Abbreviations: GLCM = Gray-level Co-occurrence Matrix, GLSZM = Gray-Level Size Zone Matrix, LoG=Laplacian of Gaussian, RLGL = Run Length Gray-Level, L=Low, H=High. Adapted from Aerts et al 2014, Coroller et al 2015

Selected Radiomic feature	**Radiomic group**	**Filter associated**	Description
Sphere Disproportionality	Shape	none	Ratio between tumor surface area and a sphere with the same volume as the tumor
Mean	Stats	Wavelet	The mean voxel intensity
Median	Stats	Wavelet	The median voxel intensity
Skewness	Stats	none	Description of the shape of the voxel intensity histogram
Kurtosis	Stats	none	Description of the shape of the voxel intensity histogram
Cluster Shade	GLCM	LoG	Measure of GLCM matrix skewness
Corr	GLCM	Wavelet , LoG	Correlation of the GLCM matrix
Entropy	GLCM	LoG	Describes the complexity of the GLCM matrix based on the number of unique voxel patterns in the tumor
Dissimilarity	GLCM	none	Describes the variation of grey level pairs in an image.
Gray Level Non Uniformity (GLN)	GLCM	Wavelet	Measures the similarity of gray level values throughout the image. Smaller values are expected if gray levels are more homogenous.
Large Area Emphasis (LRE)	GLSZM	LoG	Describes areas of connecting voxels with same value
Low Intensity Emphasis	GLSZM	Wavelet	Returns values correlated to zones with low intensity voxel
High intensity emphasis	GLSZM	Wavelet	Returns values correlated to zones with high intensity voxels
Long/Short Run Emphasis (LRE/SRE)	RLGL	LoG	Returns values based on the occurrences of long or short runs (greater or fewer voxels of similar intensity in sequence)

Table 2: Patient and treatment characteristics of patients of locally advanced NSCLC patients with pre- and post-treatment imaging reported as number of patients (% of total patients).

Patient Characteristics	**n (%)**
Age (yr)	
Median (Range)	60 (32-77)
Q1-Q3	55-66
Gender	
Male	58 (57.4)
Female	43 (42.6)
Race	
White	91 (90.1)
Other (African American, Hispanic, Asian)	10 (9.9)
ECOG Performance Status	
0	42 (41.6)
1	52 (51.5)
2	5 (5.0)
3	2 (2.0)
AJCC Stage	
IIA	2 (2.0)
IIB	7 (6.9)
IIIA	77 (76.2)
IIIB	15 (14.9)
T Stage	
T1	19 (18.8)
T2	33 (32.7)
T3	30 (29.7)
T4	19 (18.8)
N Stage	
N0	15 (14.9)
N1	8 (7.9)
N2	70 (69.3)
N3	8 (7.9)
NSCLC Histology	
Adenocarcinoma	58 (57.4)
Squamous cell carcinoma	27 (26.7)
Other*	16 (15.8)
Treatment Characteristics	
Chemotherapy	
Sequential	1 (1.0)

Induction + concurrent	13 (12.9)
Concurrent	50 (49.5)
Concurrent + Adjuvant	36(35.6)
RT only	1 (1.0)
Concurrent Chemotherapy	
Weekly carboplatin + taxol	25 (24.8)
Cisplatin + etoposide (EP 50/50)	68 (67.3)
Other	6 (5.9)
Surgery	
Lobectomy/Bilobectomy	74 (73.3)
Pneumonectomy	12 (11.9)
Wedge resection or sublobar resection	15 (14.9)
Radiation Technique	
3DCRT	87 (86.1)
IMRT	14 (13.9)
RT Dose	
Median (Range)	54 (46-70)
46-53 Gy	3 (3.0)
54 Gy	63 (62.4)
55-60 Gy	10 (9.9)
≥ 66 Gy	25 (24.8)
* NSCLC NOS (10), NSCLC with neuroendocrine morphology (2), Adenosquamous (1), Mixed NSCLC and SCLC (1), Adenoid cystic carcinoma (1), Sarcomatoid (1)	

Table 3: Treatment outcomes reported following surgical resection of locally advanced NSCLC patients with pre- and post-treatment imaging. RECIST response reported at the time of imaging prior to surgical resection.

Treatment Outcomes	Median (months)
Follow up	36.1
Overall survival	60.1
Distant metastsis	68.5
Locoregional recurrence	Not reached

RECIST response	n (%)
Complete response (CR)	1 (1.0)
Partial response (PR)	42 (41.6)
Stable Disease (SD)	56 (55.4)
Progressive Disease (PD)	2 (2.0)

Figure 3: Tumor response waterfall plot indicating percent change in total tumor diameter (a) and volume (c) for each patient in the study. Dashed line indicates 30% reduction in tumor diameter corresponding to RECIST partial response (a) and 50% median reduction in tumor volume (c). Comparison of relative changes in total tumor diameter (b) and volume (d). Diamond indicates mean change. Pathologic response is represented by red (pCR) or blue (residual disease) bars on the waterfall plots.

Abbreviations: pCR= pathologic complete response, * = p<0.05, *** = p<0.001

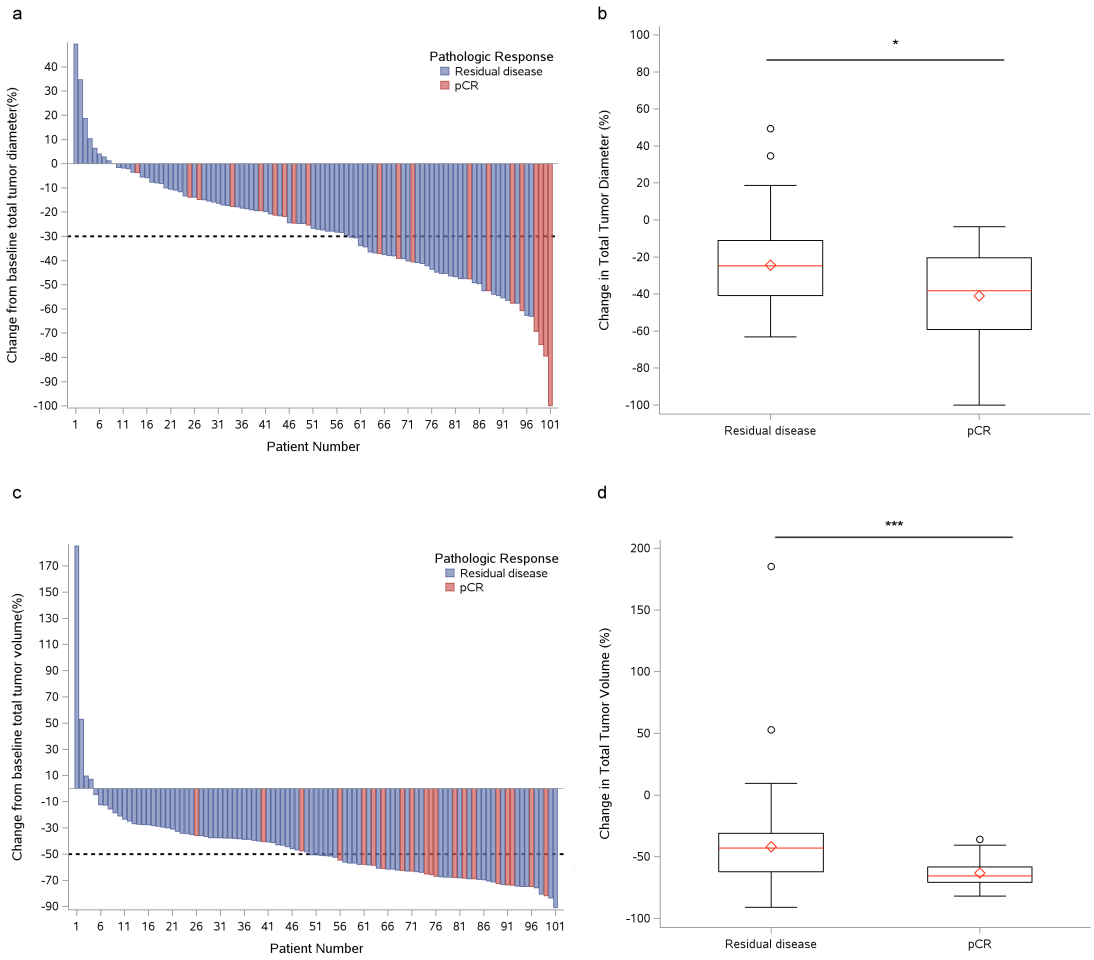

Table 4: Univariate and multivariate analysis of clinical and CT imaging variables associated with pathologic complete response (pCR). All variables are categorical except where labeled as continuous.

		Univariate			Multivariate	
	n	**OR (95% CI)**	**p**		**OR (95% CI)**	**p**
Age						
≤ 60	54	1.000				
> 60	47	1.528 (0.571-4.087)	0.399			
Gender						
Female	43	1.000				
Male	58	1.872 (0.697-5.022)	0.213			
Performance Status						
0	42	1.000				
1-3	59	1.867 (0.652-5.345)	0.245			
Race						
White	91	1.000				
Asian, African-American or Hispanic	10	1.014 (0.198-5.191)	0.987			
AJCC Stage						
IIA-IIIA	86	1.000				
IIIB	15	0.581 (0.120-2.813)	0.500			
T Stage						
T1-T2	52	1.000				
T3-T4	49	2.321 (0.839-6.425)	0.105			
N Stage						
N0-N1	23	1.000			1.000	
N2-N3	78	0.191 (0.066-0.551)	0.002		0.180 (0.052 0.621)	0.001
Histology						
Adenocarcinoma	58	1.000			1.000	0.009
Other	16	4.817 (1.189-19.521)	0.290		6.077 1.230 30.034	
Squamous cell carcinoma	27	6.234 (1.869-20.789)	0.051		6.771 1.691 27.116	
Radiation dose						
≤ 54 Gy	66	1.000				
> 54 Gy	35	1.333 (0.487-3.649)	0.575			
RECIST response						
SD/PD	58	1.000				
CR/PR	43	1.872 (0.697-5.022)	0.213			
Clinical lymph node stations involved						

0-1	36	1.000				
2	27	0.196 (0.050-0.777)	0.374			
≥3	38	0.135 (0.035-0.523)	0.087			
Imaging characteristics						
Pre-treatment total tumor volume (continuous per cm^3)		0.998 (0.993-1.004)	0.573			
Post-treatment total tumor volume (continuous per cm^3)		0.986 (0.966-1.006)	0.157			
Absolute decrease total tumor volume (continuous per cm^3)		1.001 (0.993 1.009)	0.805			
% Decrease total tumor volume (continuous per percentage point)		1.056 (1.021-1.093)	0.002		1.066 (1.022 1.111)	0.004
< 50% decrease total volume*	49	1.000				
> 50% decrease total volume	52	7.448 (2.022-27.430)	0.003			
< 65% decrease total volume †	73	1.000				
> 65% decrease total volume	28	4.601 (1.642-12.896)	0.004			
Pre-treatment primary tumor volume (continuous per cm^3)		0.999 (0.993-1.004)	0.654			
Post-treatment primary tumor volume (continuous per cm^3)		0.990 (0.974-1.007)	0.249			
% Decrease primary tumor volume (continuous per percentage point)		1.042 1.012 1.073	0.005			
Pre-treatment tumor diameter total (continuous per cm)		1.014 (0.856-1.200)	0.875			
Post-treatment tumor diameter total (continuous per cm)		0.798 (0.613-1.040)	0.095			
% Decrease tumor diameter total (continuous per percentage point)		1.035 (1.010-1.061)	0.006			
Pre-treatment primary diameter (continuous per cm)		1.027 (0.843-1.250)	0.7925			
Post-treatment primary diameter (continuous per cm)		0.884 (0.685-1.141)	0.344			
% Decrease primary tumor diameter (continuous per percentage point)		1.050 (1.015-1.087)	0.005			
*Median decrease in tumor volume						
†Upper quartile decrease in tumor volume						

Figure 4: AUC values of ROC curves modeled from logistic regression of imaging characteristics and pathologic response. Significance is indicated from random (AUC=0.5). Abbreviations: TV=tumor volume, TD=tumor diameter, * = p<0.05, *** = p<0.001

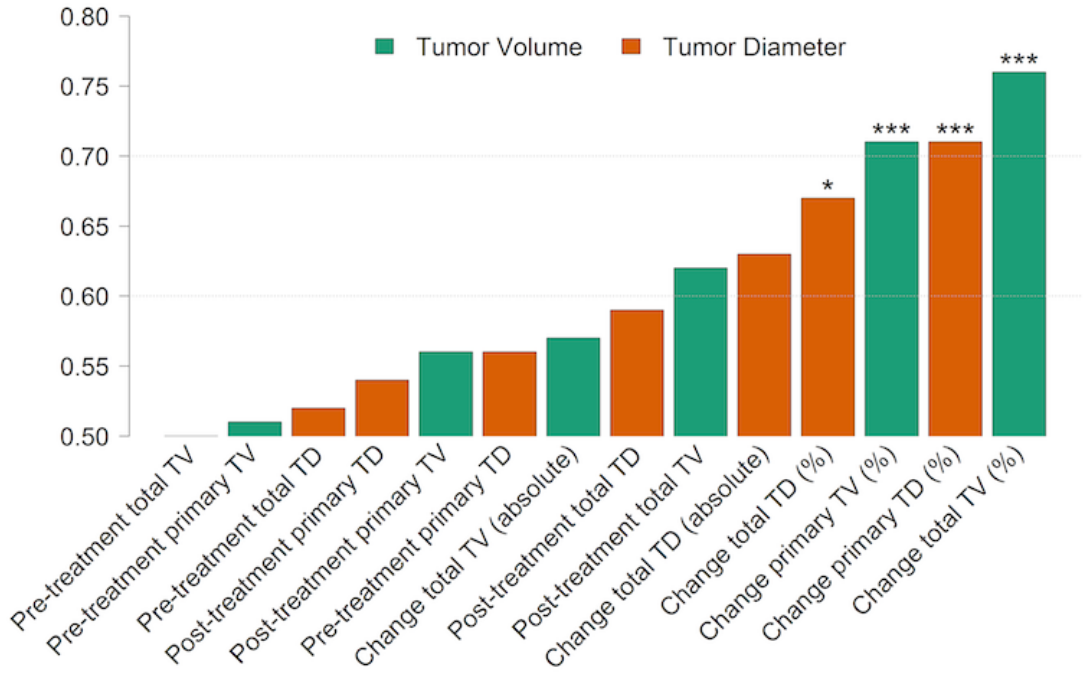

Figure 5. Kaplan Meier curves for Stage IIIA locoregional recurrence-free survival grouped by change in tumor volume (a) or RECIST response (b). Patients shown are only stage IIIa. + marks represent censored results. P-values listed using log-rank test.

Abbreviations: RECIST CR: complete response, PR: partial response, SD: stable disease, PD: progressive disease

A

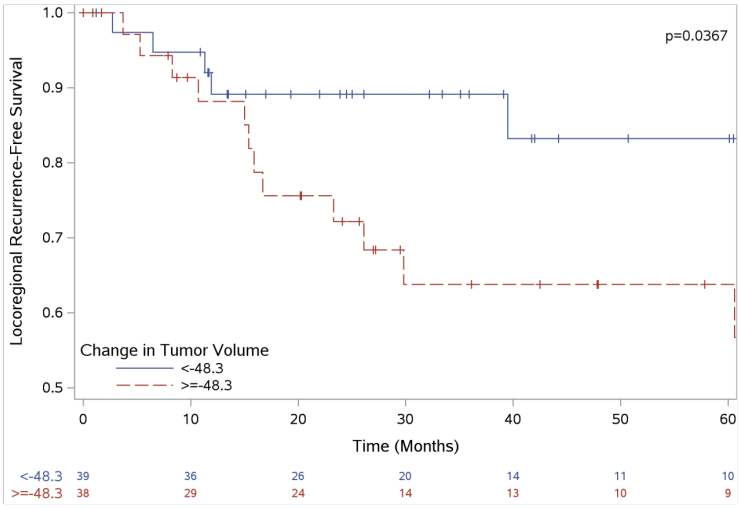

B

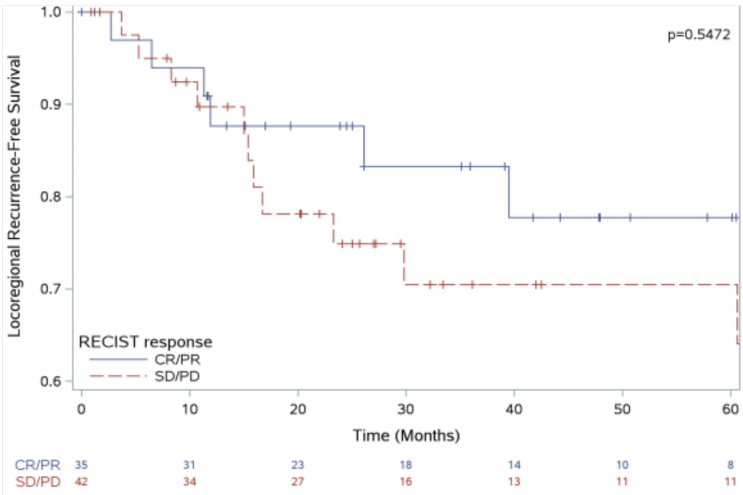

Table 5. Patient and treatment characteristics of patients of locally advanced NSCLC patients with pre-treatment imaging reported as number of patients (% of total patients).

Patient Characteristics	n (%)
Age	
Median (Range)	60.5 (32.7-77.6)
Gender	
Female	68 (53.5)
Male	59 (46.5)
Race	
American African	5 (3.9)
Asian	2 (1.6)
White	117 (92.1)
Hispanic	3 (2.4)
Histology	
Adenocarcinoma	72 (56.7)
Adenosquamous carcinoma	1 (0.8)
Squamous cell Carcinoma	32 (25.2)
Large cell Carcinoma	17 (13.4)
Large cell neuroendocrine carcinoma	2 (1.6)
Mixed NSCLC and SCLC	1(0.8)
Adenoid cystic carcinoma	1(0.8)
Other	1(0.8)
AJCC Stage	
IIA	2 (1.6)
IIB	8 (6.3)
IIIA	96 (75.6)
IIIB	21 (16.5)
Treatment Characteristics	n (%)
Treatment sequence	
Concurrent	60 (47.2)
Concurrent + adjuvant	45 (35.4)
Concurrent + adjuvant RT	2 (1.6)
Concurrent + neoadjuvant	4 (3.2)
Induction + concurrent	13 (10.2)
Induction + concurrent + adjuvant ChemoRT	1 (0.8)
RT only	1 (0.8)
Sequential	1 (0.8)
Pathologic response	
Complete response	27 (21.3)
Microscopic residual disease	33 (26.0)
Visibly residual disease	67 (52.8)

Table 6: Treatment outcomes reported following surgical resection of locally advanced NSCLC patients with pre-treatment imaging.

Treatment Outcomes	Median (months)
Follow up	41.8
Overall survival	41.7
Distant metastasisl	24.8
Locoregional recurrence	28.1

Table 7: PCA selection of primary tumor features

Pre-treatment primary tumor features
LoG sigma 3 mm 3D glcm clusProm
LoG sigma 4 mm 2D glcm homogeneity2
LoG sigma 4 mm 3D stats skewness
LoG sigma 5 mm 3D glcm entrop2
LoG sigma 5 mm 3D glszm highIntensityLarteAreaEmp
LoG sigma 5 mm 3D glszm largeAreaEmphasis
LoG sigma 5 mm 3D stats kurtosis
Shape spherDisprop
Wavelet HLL stats mean
Wavelet HLL stats rms
Wavelet LHH glcm correl1
Wavelet LHH glszm lowIntensityLargeAreaEmp
Wavelet LHH stats energy
Wavelet LHH stats range
Wavelet LLH stats range

Figure 6: Comparison of univariate AUC values for pre-treatment radiomics features against pathologic response outcomes of gross residual disease and pathologic complete response. Significance is indicated by (*) for p<0.05.
Figure created by Thibaud Coroller and used with permission.

Figure 7: Comparison of concordance indices (CI) for pre-treatment radiomics features against outcomes of OS, DM, LRR. Significance is indicated by (*) for p<0.05.
Figure created by Thibaud Coroller and used with permission.

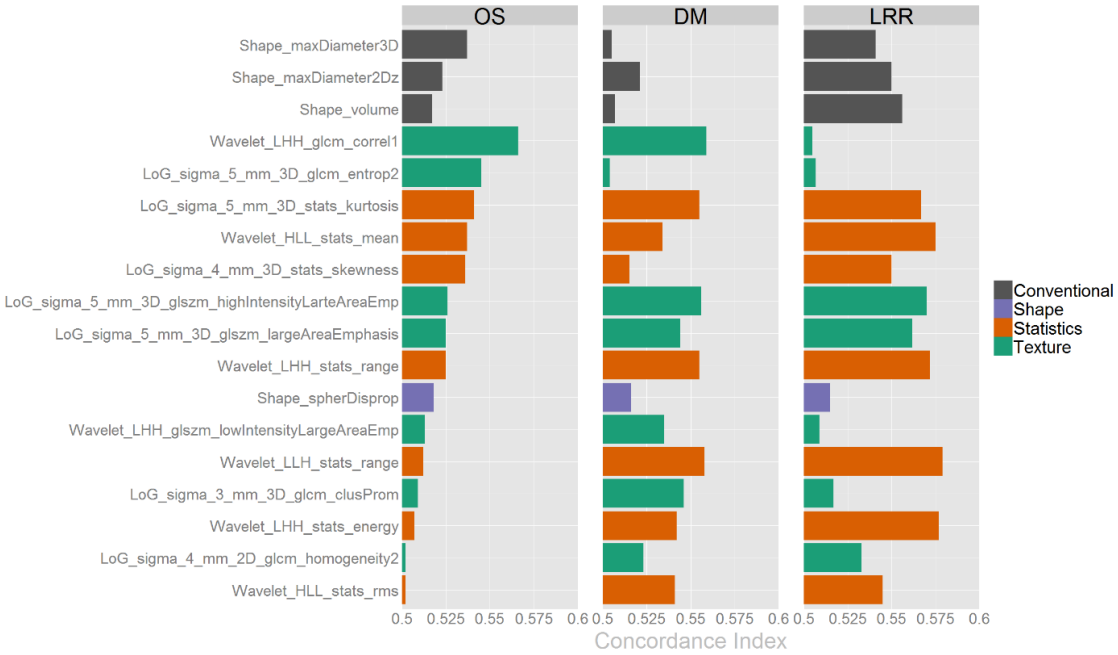

Table 8. Patient and treatment characteristics of patients of locally advanced NSCLC patients with pre- and post-treatment imaging reported as number of patients (% of total patients). Only patients with lymph node segmentation were included in this table.

Patient Characteristics	**n (%)**
Age (yr)	
Median (Range)	60 (32-75)
Q1-Q3	53-65
Gender	
Male	22 (30.1)
Female	51 (69.9)
Race	
White	66 (90.4)
Other (African American, Hispanic, Asian)	7 (9.6)
ECOG Performance Status	
0	30 (41.1)
1	39 (53.4)
2	4 (5.5)
AJCC Stage	
IIIA	61 (83.6)
IIIB	12 (16.4)
T Stage	
T1	18 (24.7)
T2	32 (43.8)
T3	17 (23.3)
T4	6 (8.2)
N Stage	
N2	66 (90.4)
N3	7 (9.6)
NSCLC Histology	
Adenocarcinoma	48 (65.8)
Squamous cell carcinoma	16 (21.9)
Other*	9 (12.3)
Treatment Characteristics	
Chemotherapy	
Induction + concurrent	9 (12.3)

Concurrent	37 (50.7)
Concurrent + Adjuvant	27 (37.0)
Concurrent Chemotherapy	
Weekly carboplatin + taxol	17 (23.3)
Cisplatin + etoposide (EP 50/50)	51 (69.9)
Other	5 (6.8)
Surgery	
Lobectomy/Bilobectomy	57 (78.1)
Pneumonectomy	6 (8.2)
Wedge resection or sublobar resection	10 (13.7)
Radiation Technique	
3DCRT	63 (86.3)
IMRT	10 (13.7)
RT Dose	
54 Gy	49 (67.1)
55-60 Gy	8 (11.0)
≥ 66 Gy	16 (21.9)

Table 9: Treatment outcomes reported following surgical resection of locally advanced NSCLC patients with pre- and post-treatment imaging. Only patients with lymph node segmentation were included in this table.

Treatment Outcomes	Median (months)	1 year	3 year
Follow up	36		
Overall survival	78	85%	68%
Distant recurrence	68.6	23%	38%
Locoregional recurrence	Not reached	12%	28%

Treatment Outcomes
Median (months)
1 year
3 year

Follow up
36

Overall survival
78
85%
68%

Distant recurrence
68.6
23%
38%

Locoregional recurrence

NR*

Figure 8: Comparison of concordance indices (CI) for total tumor volume, total lymph node volume and mediastinal lymph node volume against outcomes of distant metastasis (DM), locoregional recurrence (LRR), and overall survival (OS). Significance from random is indicated by (*) for $p<0.05$.

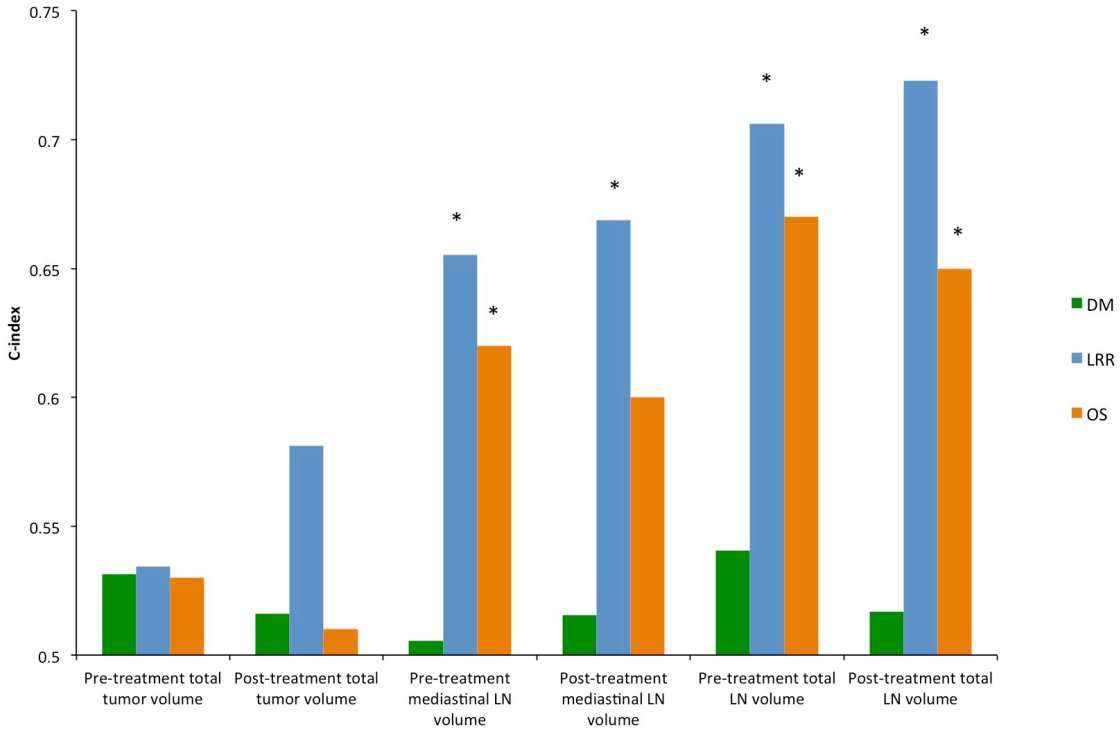

`**Figure 9:** Kaplan Meier curves for patients with N2 nodal disease. Locoregional recurrence grouped by pre-treatment N2 nodal volume (a) or post-treatment nodal volume (c). Overall survival grouped by pre-treatment N2 nodal volume (b) or post-treatment nodal volume (d). + marks represent censored results. P-values listed using log-rank test.

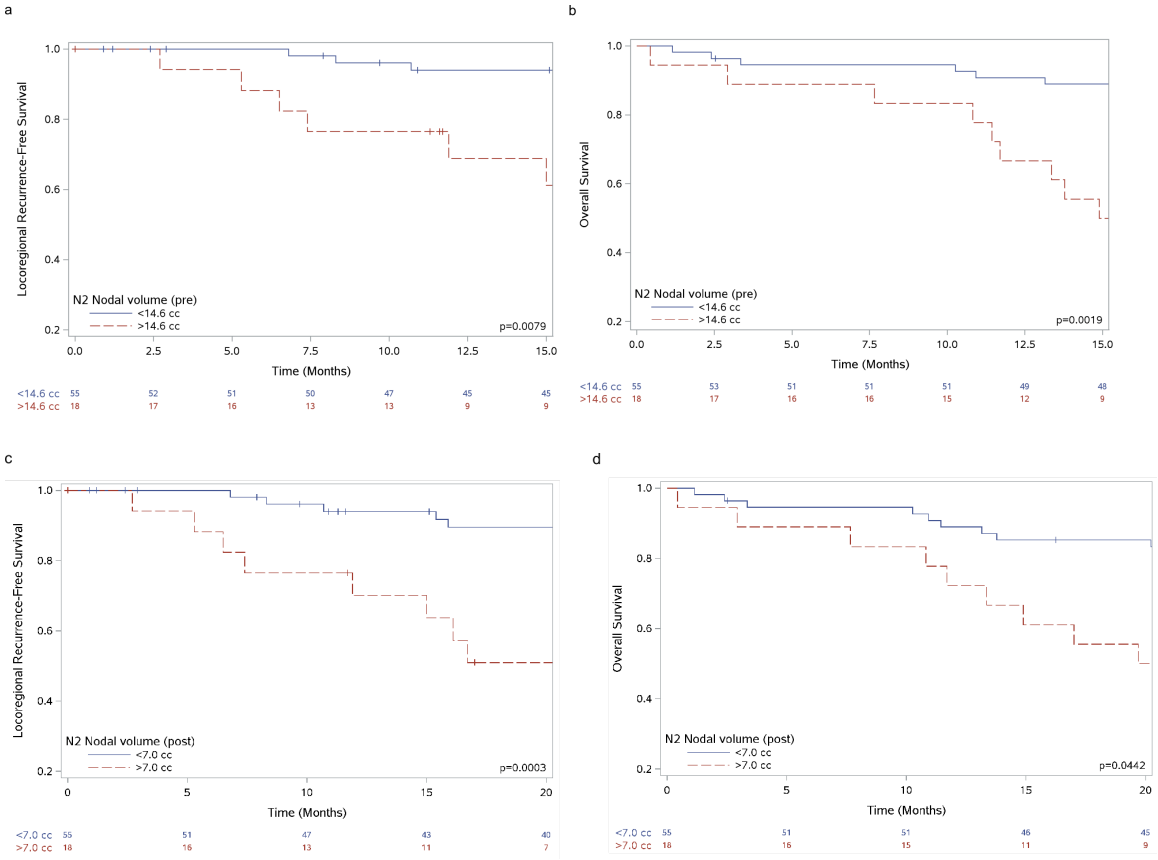

Table 10: PCA selection of lymph node features

Pre-treatment lymph node features	Post-treatment lymph node features
Unique features	
GLCM clusProm	LoG sigma 4 mm 3D rlgl shortRunHighGrayLevEmpha
GLCM inverseVar	LoG sigma 5 mm 2D glcm clusShade
LoG sigma 5 mm 3D glcm invDiffnorm	LoG sigma 5 mm 2D rlgl longRunEmphasis
LoG sigma 4 mm 2D glcm correl1	LoG sigma 5 mm 3D glcm infoCorr2
LoG sigma 5 mm 2D glszm highIntensityLargeAreaEmp	LoG sigma 5 mm 2D glszm zonePercentage
LoG sigma 5 mm 3D glszm intensityVariability	LoG sigma 5 mm 3D glszm intensityVariability
LoG sigma 5 mm 2D glszm smallAreaEmphasis	LoG sigma 5 mm 3D glszm highIntensityLarteAreaEmp
LoG sigma 5 mm 3D glszm lowIntensityEmphasis	Wavelet LLH glcm sumVar
Shape spherDisprop	Wavelet HLL glcm contrast
Stats kurtosis	Wavelet LLL glcm clusShade
Wavelet LLL glcm dissimilar	Wavelet HHL stats MeanIntensity
Wavelet LHL stats md	Wavelet HHL stats var
Wavelet HLH glszm largeAreaEmphasis	Wavelet HHH stats uniformity
Wavelet LLL glcm infoCorr2	Wavelet LLL stats kurtosis
Common Features	
Wavelet LLH stats std	Wavelet HLH stats std
Wavelet LLL glcm inverseVar	Wavelet LLL glcm inverseVar

Figure 10: Comparison of pre-treatment lymph node radiomics features c-indices for locoregional recurrence, distant recurrence, and overall survival. (*) indicates p-values <0.05.

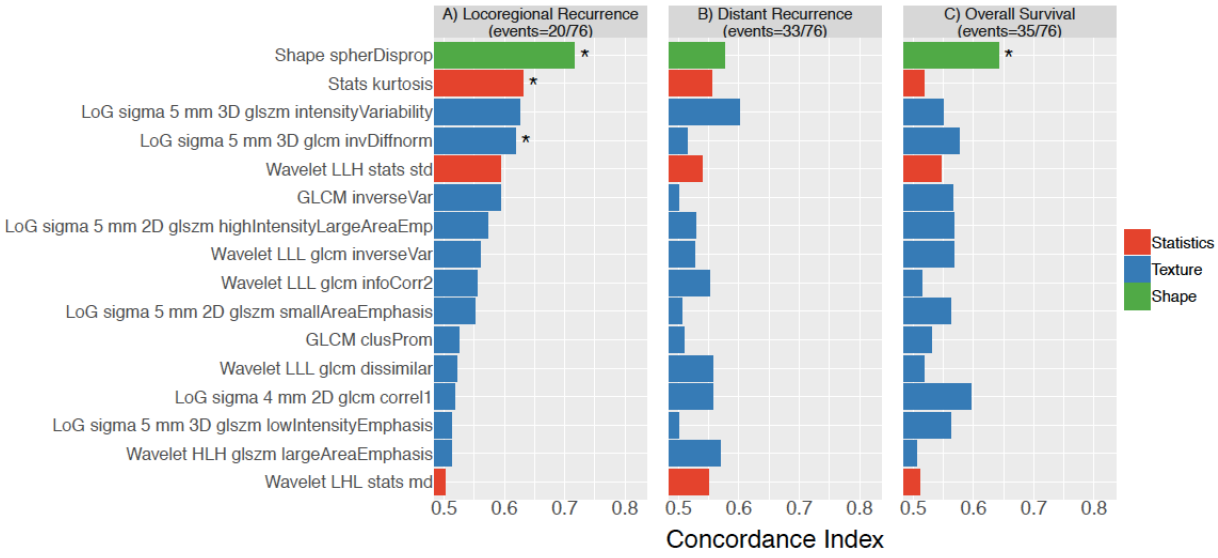

Figure 11: Comparison of post-treatment lymph node radiomics features c-indices for locoregional recurrence, distant recurrence, and overall survival. (*) indicates p-values <0.05.

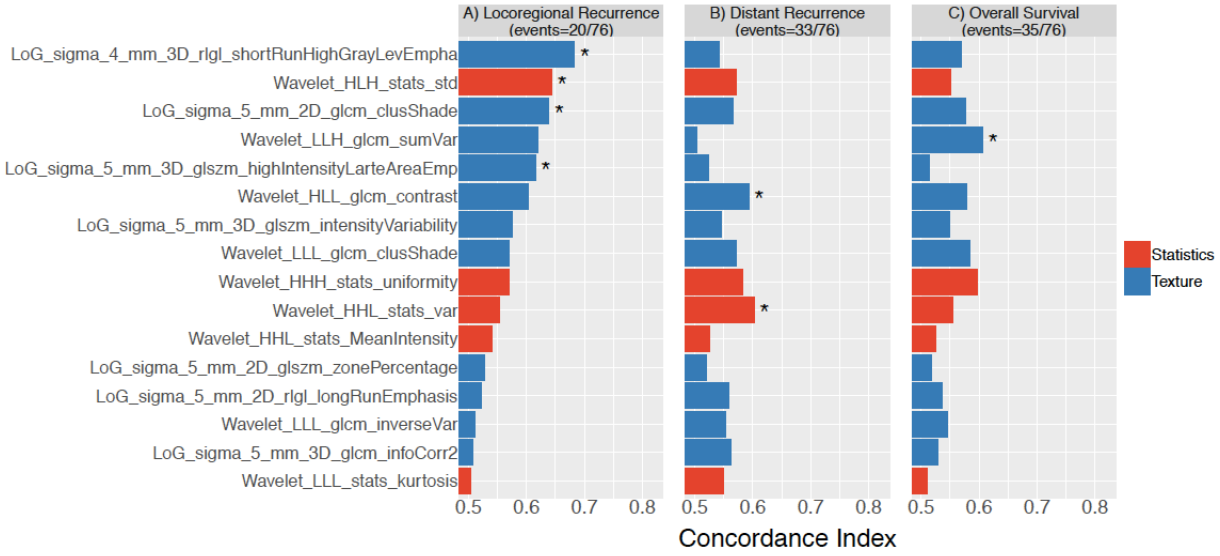

Figure 12: Comparison of delta lymph node radiomics features c-indices for locoregional recurrence, distant recurrence, and overall survival. (*) indicates p-values <0.05.

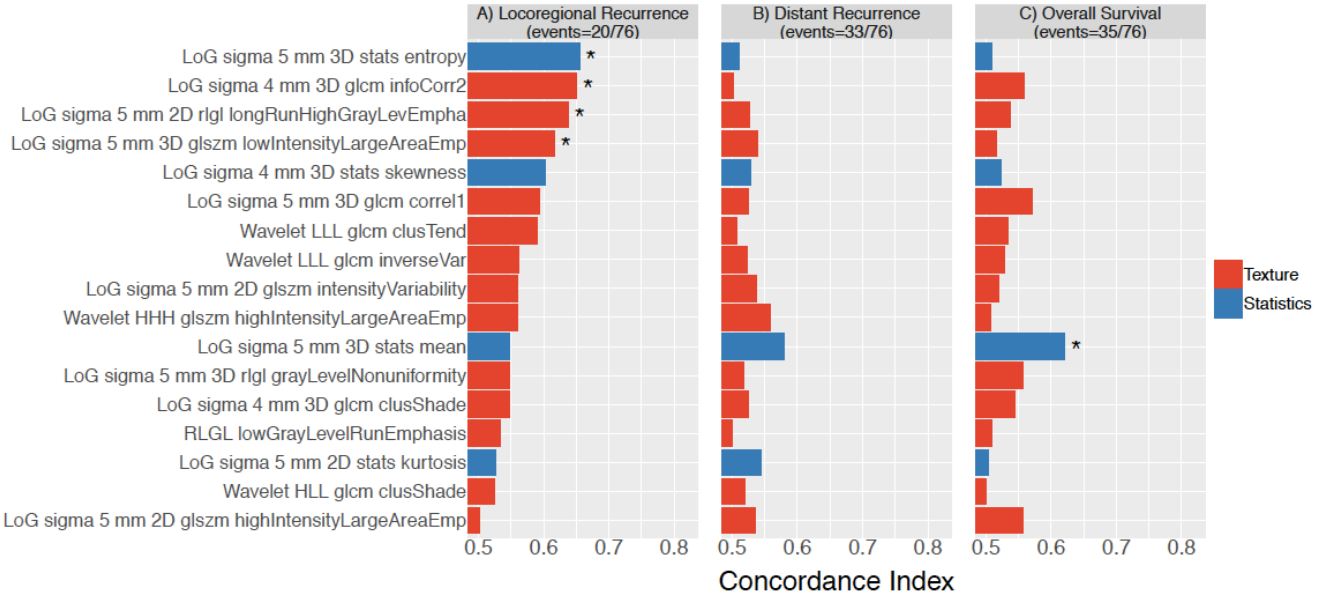

Table 11: SBRT patient and treatment characteristics reported as number of patients (% of total patients).

Patient Characteristics	n (%)
Age (yr)	
Median (Range)	74 (46-93)
Gender	
Male	46 (46.5)
Female	53 (53.5)
Race	
White	91 (91.9)
Other (African American, Hispanic, Asian)	8 (8.1)
ECOG Performance Status	
0	17 (17.2)
1	46 (46.5)
2	28 (28.3)
3-4	8 (8.1)
AJCC Stage	
IA	78 (78.8)
IB	16 (16.2)
II-IV	5 (5.1)
T Stage	
T1a	51 (51.5)
T1b	29 (29.3)
T2	18 (18.2)
T3	1 (0.1)

N Stage	
N0	99 (100)
Histology	
Adenocarcinoma	46 (46.5)
Squamous cell carcinoma	23 (23.2)
NSCLC NOS	14 (14.1)
No pathology specimen	15 (15.2)
Treatment Characteristics	
SBRT fractions	
3	62 (62.6)
4	2 (0.2)
5	35 (35.4)
RT Dose per fraction	
Median (Range)	18 (10-18)
11	12
12	19
18	62
Other	6
Total RT dose	
Median (Range)	54 (48-60)

Table 12: SBRT patient treatment outcomes

Treatment Outcomes	Median (months)	1 year	3 year
Follow up	20.1 (1.25-51.4)		
Overall survival	28.5	89.2%	35.2%
Locoregional recurrence	39.2	22.5%	37.9%
Distant recurrence	NR	19.9%	33.9%

Figure 13: Comparison of CBCT volumetric feature c-indices for LRR. (*) indicates p-values <0.05.

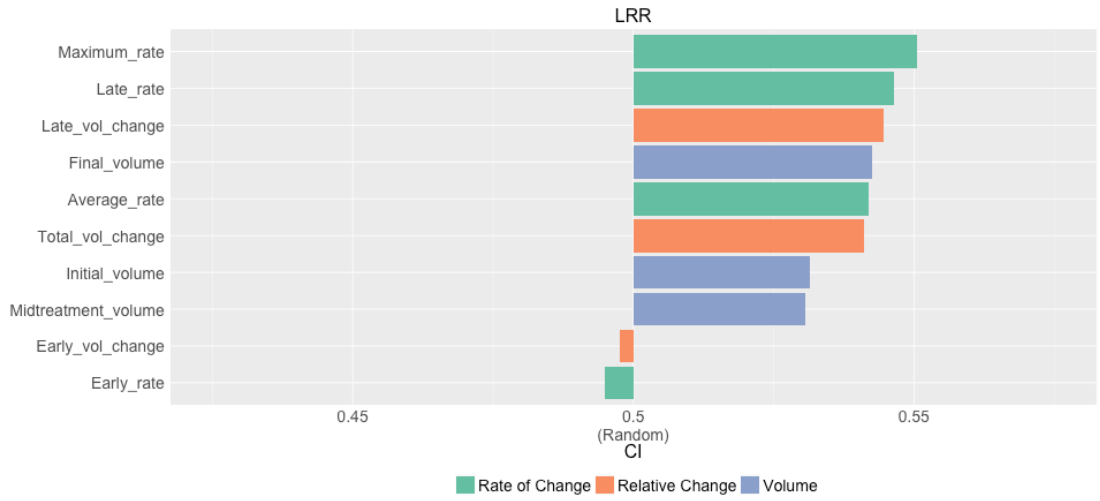

Figure 14: Comparison of CBCT volumetric feature c-indices for any recurrence. (*) indicates p-values < 0.05.

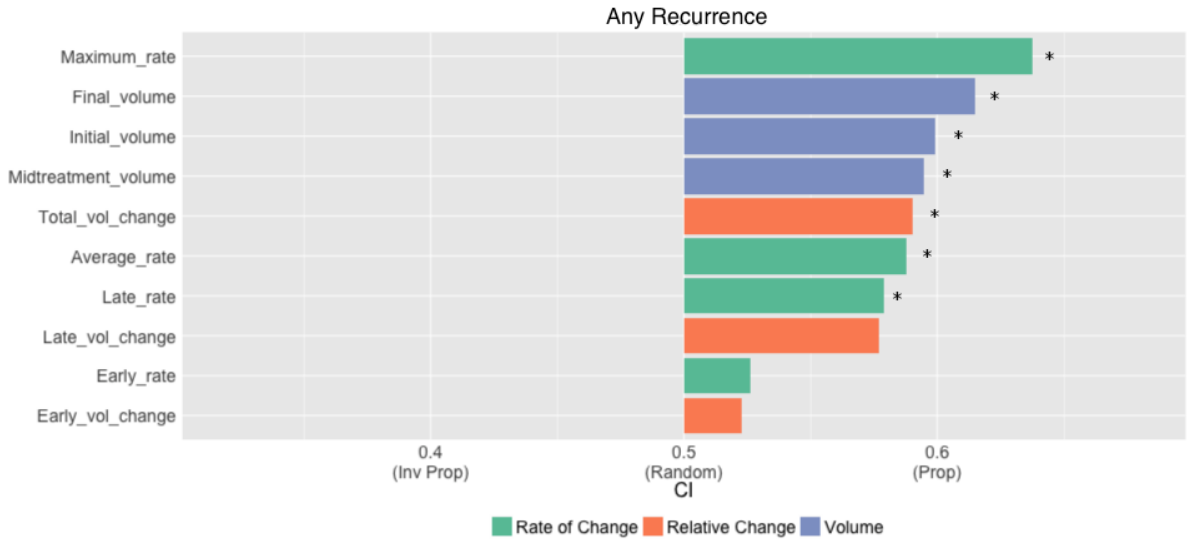

Figure 15: Comparison of CBCT volumetric feature c-indices for OS. (*) indicates p-values <0.05.